Geophys. J. R. astr. Soc. (1980) **60**, 209–244

High-frequency seismic wave propagation in western South America along the continental margin, in the Nazca plate and across the Altiplano

Douglas S. Chinn, Bryan L. Isacks and
Muawia Barazangi* *Department of Geological Sciences, Cornell University, Ithaca, New York 14853, USA*

Received 1979 June 20; in original form 1978 November 6

Summary. High-frequency shear waves (0.5–2 Hz) recorded at regional distances at WWSSN stations in western South America are classified according to their apparent velocity and frequency/amplitude character. For propagation paths crossing any given region, the observations are abundant and consistent.

Sn is not observed at distances beyond about 15.5° along paths in the eastern part of the relatively young (Eocene) oceanic Nazca plate. This observation does not appear to be related to any specific tectonic or structural feature along the propagation paths. In contrast, *Sn* is observed at distances beyond about 25° in the older (Jurassic–Cretaceous) parts of the western Pacific and western Atlantic oceanic plates and to distances of over 40° in continental shield regions. One interpretation of these and other data is that the maximum distance over which *Sn* is observed increased with the thickness of the lithosphere. The disappearance of *Sn* in the Nazca plane is quite sharp, occurring between 15 and 16°. Such a phenomenon cannot be explained by simple attenuation mechanisms.

Lateral variations in *Sn* propagation occur beneath the Altiplano, a high plateau in the central Andes. Two types of seismograms imply inefficient *Sn* propagation: one shows no *Sn*, implying an average low-Q along the path; the other has a complex ringing character suggesting a large amount of scattering along the path. *Sn* is also observed to propagate efficiently across some parts of the Altiplano, which would usually imply high-Q material in the mantle wedge that separates the South American plate from the descending Nazca plate. However, because the dip of the descending Nazca plate beneath the Altiplano is only about 30°, it is possible that these *Sn* waves are actually refracted along the descending plate instead of travelling mainly through the mantle wedge.

Sn has a velocity of about 4.5 km/s along western South America. *Sn* travelling in the oceanic Nazca plate converts efficiently into *Lg* travelling

* Present address: Faculty of Earth Sciences, King Abdulaziz University, Jeddah, Saudi Arabia.

in the continental crust where the crust thickens beneath the Andes. No reverse *Lg* to *Sn* conversion is observed. Lateral variations in *Lg* propagation appear to be related to the orientation of the path relative to the structural trend of the Andes rather than to anomalous regions in the continental crust. It appears that *Lg* propagates efficiently only when the direction of propagation is approximately parallel to the strike of the Andes.

Introduction

The seismic phase *Sn* consists of high-frequency shear waves that travel mainly in the lithosphere within the high-velocity lid between the Moho and the upper mantle low-velocity zone. Studies of the propagation of *Sn* have proven to be quite useful in mapping the continuity and areal extent of the lithosphere and, to some degree, in mapping lateral variations in lithospheric structure (e.g. Molnar & Oliver 1969; Barazangi & Isacks 1971; Hart & Press 1973; Huestis, Molnar & Oliver 1973). Detailed *Sn* studies have provided much information about the structure of oceanic island arcs (e.g. Oliver & Isacks 1967; Mitronovas, Isacks & Seeber 1969; Aggarwal, Barazangi & Isacks 1972; Barazangi, Isacks, Dubois & Pascal 1974; Rial 1976). The terms *Lg* and *Sg* both refer to high-frequency shear waves in the continental crust. When the first arrival travels from the source to the station as a direct ray, i.e. at short distances, the waves are called *Sg*. For large epicentral distances relative to the thickness of the crust, the waves travel to the station as normal modes and are called *Lg*. For the range of distances encountered in this paper, we used these two terms interchangeably.

This paper reports a comprehensive survey of high-frequency shear wave propagation in the region of western South America where the oceanic Nazca plate is descending beneath a major continental plate. As in previous studies of *Sn*, our data consist of short period records made at stations of the World-Wide Standardized Seismograph Network (WWSSN) and thus considers the propagation of seismic waves primarily in the band of frequencies between 0.5 and 2 Hz. Three results of this survey contrast markedly with the results of previous surveys of oceanic island arc regions in the southwest Pacific. Firstly, although *Sn* clearly propagates through the oceanic Nazca plate, the distances over which the phase is observed and the velocity of the phase are significantly less than those found in the older, and presumably thicker, oceanic plates of the western Pacific and western Atlantic. Secondly, the large change in crustal thickness across the continental margin appears to be especially conducive to the conversion of oceanic *Sn* into crustal shear waves (*Lg* or *Sg*), which propagate efficiently in the continental crust (Isacks & Stephens 1975). High frequency shear waves, though, have not been observed to propagate efficiently in oceanic crust (Barazangi, Oliver & Isacks 1978). Thirdly, propagation 'behind' the South American subduction zone, i.e. through the wedge-shaped region of mantle and crust above the descending Nazca plate, is not simply characterized by the complete absence of high-frequency shear waves that is observed behind southwest Pacific island arcs. Instead, high-frequency seismic waves are observed along certain paths across the wedge as are waves characterized by a large amount of scattering. These complexities, in addition to the segmentation of the descending plate into two nearly flat segments (about 10° dip) in central Peru and in central Chile plus a steeper segment (about 30° dip) in southern Peru–northern Chile (Barazangi & Isacks 1976), make the interpretation of these data difficult and somewhat ambiguous compared to similar studies in island arc regions.

This survey focuses on high-frequency shear waves generated by shallow- and intermediate-depth earthquakes. Propagation from deep South American earthquakes is discussed by Isacks & Barazangi (1973) and Snoke, Sacks & Okada (1974). Our data consist of short-

period seismograms of five WWSSN stations in Peru, Bolivia, and Chile. The abundant seismicity in western South America provides numerous propagation paths. The examination, classification, and analysis of the varieties of short-period shear waves that travel along these paths are the basic contributions of this paper. Compressional arrivals are also included, but the variations in appearance and frequency content are not as marked or consistent as those for shear waves. Most of the results of this paper pertain to *Sn* and to a much smaller extent to *Lg*/*Sg*.

Many papers have been written to explain the variations in the properties of the oceanic lithosphere with the age of the plate. The most general conclusion of these studies is that the oceanic lithosphere seems to cool and thicken with age (e.g. Sclater, Lawver & Parsons 1975; Yoshii, Yoshiteru & Ito 1976). Other authors have also found a correlation between higher seismic wave velocities and the age of the oceanic plate (e.g. Hart & Press 1973; Kausel, Leeds & Knopoff 1974; Leeds, Knopoff & Kausel 1974; Forsyth 1975; Leeds 1975; Duschenes & Solomon 1977). Presumably this systematic increase in velocity with age is directly related to the relatively lower temperatures and greater thicknesses of the older parts of the oceanic plates. Most of the previous studies of oceanic *Sn* were made on the relatively old parts of the western Pacific and western Atlantic plates (≈ 100 m yr). In these regions, *Sn* has velocities of 4.7 to 4.8 km/s and can be observed to distances greater than 25° on short-period instruments of the WWSSN. In the older continental shield regions, *Sn* has velocities comparable to those found in old oceanic plates but can be observed to distances greater than 40° (Båth 1966). The Nazca plate along western South America is about 50 m yr old. *Sn* has a relatively low velocity of about 4.5 km/s and is not observed at distances greater than 16° in this part of the plate. The disappearance of *Sn* occurs rather abruptly between 15 and 16°, which makes it difficult to understand this cutoff phenomenon in terms of the usual models of attenuation. However, little has been reported previously on exactly how *Sn* is attenuated as a function of distance. Our results suggest that both the cutoff distance as well as the velocity of oceanic *Sn* increase with the age of the plate.

Isacks & Stephens (1975) observed the efficient conversion of oceanic *Sn* into continental *Lg* at the eastern margin of North America where there is a large gradient in crustal thickness. In western South America the thickness of the crust changes from about 7 km seaward of the trench (Whitsett 1975) to perhaps about 70 km beneath the Altiplano, the high plateau in the central Andes (James 1971). In our study we found several different cases of conversion along propagation paths that cross regions of marked crustal thickening.

Behind several of the island arcs in the western Pacific are active marginal basins. The wedge-shaped upper mantles beneath these basins and above the descending plates have been inferred to have elevated temperatures and possible partial melting (e.g. Oxburgh & Turcotte 1970; Karig 1971; Toksoz, Sleep & Smith 1973). High-frequency seismic waves passing through these upper mantle wedges are severely attenuated (e.g. Barazangi & Isacks 1971). The Altiplano is a broad, high plateau in the central Andes. Its areal extent closely correlates with the relatively steeply dipping ($\approx 30°$) descending plate segment in southern Peru–northern Chile. From its location behind the South American subduction zone, the Altiplano might be proposed as a continental analogy to active marginal basins found behind island arcs. In this analogy, the Altiplano and an active marginal basin represent different responses, one primarily uplift and the other extentional rifting, to the heating and mobilization of the upper mantle by the descending plate.

Data from refraction work (Dept. of Terrestrial Magnetism staff 1970; Ocola & Meyer 1972), electrical conductivity studies (Schmucher 1969), and seismic wave attenuation (Barazangi, Pennington & Isacks 1975) have implied that parts of the uppermost mantle and

crust beneath the Altiplano are extremely hot and perhaps partially melted. This study examines a large number of paths across the Altiplano. Although the Altiplano is for the most part a region across which shear wave propagation is very poor, especially in the northern part near the inferred tear in the descending plate, the propagation is quite complex compared to that across marginal basins of the southwestern Pacific.

Across the regions north and south of the Altiplano where the Benioff zone has a very gentle dip ($\approx 10^{\circ}$), the propagation of *Sn* is uniformly very efficient. This result supports the models developed by Isacks & Molnar (1971), Sykes (1972), Stauder (1975) and Barazangi & Isacks (1976), that the subducted Nazca plate is nearly horizontal beneath the continental plate and forms a double-layered lithospheric structure with little or no wedge of asthenospheric material in between.

A complete analysis of lateral variations in the propagation of *Lg* was not done for two reasons. Firstly, the number of observations of *Lg* was much smaller than the number for *Sn*. Secondly, lateral variations in the propagation of *Lg* were not as pronounced and consistent as those observed for *Sn*.

Data and method of analysis

The data used in this study consist of short-period WWSSN seismograms produced by South American events that occurred between December 1963 and December 1974. The locations and origin times of the events were taken from the Bulletin of the International Seismological Centre (ISC) and the Preliminary Determination of Epicenters (PDE) listing of the National Earthquake Information Service. Five WWSSN stations were used: NNA (Nãna, Peru), ARE (Arequipa, Peru), LPB (La Paz, Bolivia), ANT (Antofagasta, Chile), and PEL (Peldehue, Chile).

About 3000 seismograms were collected and divided into about 10 groups according to the location of the path between the source and receiver. Each group was then analysed as a set. For example, one group contains all earthquakes located in the Benioff zone and recorded at a particular station since the paths were mainly confined to the descending plate. Another group contains all earthquakes located seaward of the trench, since the paths mainly traverse the sub-oceanic parts of the Nazca plate. All groups which contain paths mainly confined to the sub-oceanic Nazca plate are called profiles. These groups are discussed in detail in the following sections.

Each seismogram was examined for high-frequency seismic wave arrivals. The times of the beginnings of the arrivals were then used to identify the arrivals according to the velocities given in Table 1. The identifications are based on ranges of velocities of *Pn, Pg, Sn, Lg* and *Sg* commonly found in other areas. For paths lying mainly in the Nazca plate or along the continental margin, reduced travel-time versus distance graphs were made for both the shear and compressional arrivals.

Table 1. Approximate arrival velocities and associated seismic phases

Velocity (km/sec)	Associated Seismic Phase
8.0	Pn
6.7	Pg
4.5–4.6	Sn
3.8–4.4	"early Lg"
3.6	Lg
3.5	"late Lg"

Table 2. Categories of high-frequency shear arrivals.

Number	Symbol	Description
1	■	Sn only
2	□	no high-frequency shear arrivals
3	▼	Sn and "early Lg"
4	▽	"early Lg" only
5	●	Sn and Lg
6	○	Lg only
7	◆	Sn and "late Lg"
8	◇	"late Lg" only
9	◪	"indeterminant" waves consisting of a high-frequency energy build up beginning before the normal Sn arrival time and continuing through it
10	◐	"indeterminant" waves but with a distinct Lg arrival
11	◪	"highly scattered" P waves with no strong S arrival produced by shallow sub-Andean sources located near ARE and recorded only at this station
12	◥	special kind of "indeterminant" waves observed only at ARE from intermediate-depth sources north of the station

Next, the seismograms were classified according to the character of the shear wave arrivals in one of the 12 categories as shown in Table 2. Envelope A in Fig. 1 represents seismograms recording only *Sn* (No. 1 in Table 2), or no high-frequency shear arrivals (No. 2). Envelope B represents seismograms recording *Sn* and 'early *Lg*' phases (No. 3), i.e. high-frequency shear arrivals having a velocity less than the *Sn* velocity but greater than the *Lg* velocity, or only 'early *Lg*' arrivals (No. 4). Envelope C represents seismograms recording *Sn* and *Lg* (No. 5) or only *Lg* (No. 6). Envelope D represents seismograms recording *Sn* and 'late *Lg*' (No. 7) or only 'late *Lg*' (No. 8). Seismograms showing 'indeterminant' waves alone (No. 9) or 'indeterminant' waves with a distinct *Lg* arrival (No. 10) are represented by Envelope E. The manner of the energy build-up from the first arrival is quite variable. In all cases, however, there is a high-frequency energy build-up that begins before and continues through the expected *Sn* arrival time. Finally, there are two special types of seismograms observed at ARE. Envelope F is recorded from shallow sub-Andean events located to the northwest of the station between 2 and 7° away (No. 11). Envelope F is a time compressed version of Envelope E, i.e. in each case the seismogram is characterized by an emergent wavetrain spread out between the time of the *P*-wave arrival and a time corresponding to the group velocity of crustal shear waves. No clear phases are seen. These seismograms probably indicate a large amount of scattering in the propagation. Envelope G is recorded from intermediate-depth events located in central Peru about 8.5° north of the station (No. 12). These events produced a special sub-class of 'indeterminant' waves in which a secondary arrival with a velocity greater than 4.5 km/s can be picked. The paths from these events to ARE must all pass near the inferred tear in the descending Nazca plate beneath southern Peru. The epicentres of the earthquakes in each group were then plotted on Mercator projection maps using the appropriate symbols in Table 2. Finally, interpretations of the seismogram groups were made for the various regions in western South America.

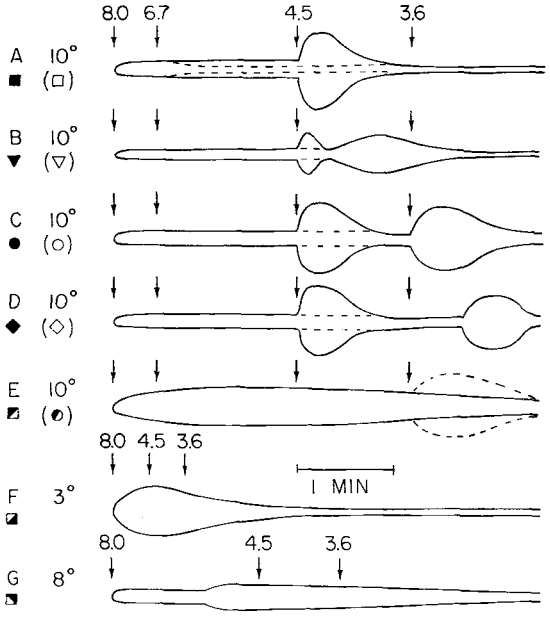

Figure 1. Envelopes of typical seismograms that represent all the different characteristics of records observed in this paper. The key to the symbols to the left of the envelopes is in Table 2. Symbols in parentheses correspond to the dashed line envelopes. The high-frequency shear wave arrivals are classified as follows: A = *Sn* (or no high-frequency shear waves as represented by the dashed lines); B = *Sn* and 'early *Lg*' (or only 'early *Lg*'); C = *Sn* and *Lg* (or only *Lg*); D = *Sn* and 'late *Lg*' (or only 'late *Lg*'); E = 'indeterminant' waves (or 'indeterminant' waves and *Lg*); F = 'highly scattered' waves produced by shallow-depth sources near ARE, and G = a special kind of 'indeterminant' waves produced by intermediate-depth sources located to the north-northwest of ARE.

The classification scheme illustrated in Table 2 and Fig. 1 characterizes all of the short-period WWSSN seismograms recorded from western South American earthquakes and is the basic contribution of this paper.

The conversion of *Sn* into *Lg* along western South America

IDENTIFYING HIGH-FREQUENCY *P* AND *S* PHASES

Fig. 2 shows some typical seismograms produced by shallow sources located along the contact zone between the overriding and descending plates. A map summarizing the data from these sources for paths which lie mainly in the Nazca plate or along the continental margin is shown in Fig. 3. The data can be divided into six groups or profiles according to the locations of the sources relative to the stations. The six profiles are NNA-south, ARE-north, ARE-south, ANT-north, ANT-south, and PEL-north. Also, data for shallow intraplate earthquakes seaward of the trench were grouped together into a profile called NAZCA (Fig. 4). Reduced travel-time versus distance is plotted for the arrivals observed on these profiles in Figs 5–8.

The reduced travel-time of the high-frequency shear wave arrivals (Figs 5 and 6) are not as simply interpreted as those found in continental shield areas. For example, Brune & Dorman (1963) could interpret all of the high-frequency shear arrivals in the Canadian shield as either an *Sn* arrival with a velocity of about 4.7 km/s or an *Lg* arrival with a velocity

of about 3.7 km/s. There, *Sn* travels mainly in the upper mantle, whereas *Lg* travels in the crust. The graphs of the four profiles in Fig. 5 show a clear series of arrivals that have a velocity of about 4.5 km/s (shown as squares). The maps in Figs 3 and 4 show that the paths for these data lie mainly in the Nazca plate. Thus, these arrivals are interpreted to be *Sn* phases travelling in the Nazca plate.

However, the pattern of the remaining data in Fig. 5 (shown as circles) cannot be simply interpreted as *Lg*/*Sg* arrivals, except possibly those in the ARE-south profile for distances between about 7 and 11° which have an apparent velocity of about 3.6 km/s. If the arrivals with a velocity of about 3.6 km/s on the NNA-south profile between 12 and 21° were *Lg*, this would imply propagation of *Lg* along an oceanic path. However, *Lg* has been shown not to propagate in oceanic crust elsewhere (e.g. Oliver, Ewing & Press 1955; Barazangi *et al.* 1978). The graphs of the three profiles in Fig. 6 show few *Sn* arrivals, but a rather large number of arrivals with velocities of about 4.0 km/s. However, there is no high-frequency phase known to travel with a velocity of 4.0 km/s.

Reduced travel-time versus distance graphs for compressional arrivals are shown in Figs 7 and 8. The graphs for compressional arrivals have characteristics similar to the corresponding graphs for shear arrivals. The graphs of the four profiles in Fig. 7 show a clear series of arrivals out to a distance of about 16° that have a velocity of about 8.0 km/s (shown as squares). These arrivals are probably *Pn* phases. Arrivals from distances beyond 16° with velocities greater than about 8.0 km/s are interpreted to be the normal mantle *P* phase. Compressional arrivals with a velocity of about 6.75 km/s in profile ARE-south (shown as circles in Fig. 7) can be interpreted to be *Pg* phases. Compressional arrivals in Fig. 8 show much scatter and cannot be interpreted as *Pn* or *Pg* phases. More careful analysis of the data show that the existence of arrivals that do not approximately trace out a line can be simply explained by whether or not the paths of the arrivals cross regions of large gradients in crustal thickness.

PROPAGATION PATHS FROM SHALLOW PERUVIAN COASTAL SOURCES TO AREQUIPA (ARE)

The graph for high-frequency shear arrivals for profile ARE-north in Fig. 6 appears to have no *Sn* or *Lg* arrivals. The arrivals for this profile are too slow to be *Sn* phases and too fast to be *Lg* phases (see seismogram No. 6 in Fig. 2). We labelled such arrivals as 'early *Lg*' phases. Since no high-frequency shear phases other than *Sn* and *Lg* have been reported for other continental areas, it is plausible to hypothesize that these 'early *Lg*' phases are due to either *Sn* to *Lg* or *Lg* to *Sn* conversion. The sources that produced these waves are shallow-depth earthquakes located northwest of ARE (Fig. 3). Since *Lg* may not propagate more than 200 km in oceanic crust (e.g. Barazangi *et al.* 1978), the most plausible explanation for these waves is that they represent *Sn* to *Lg* conversion.

Assuming this type of conversion, calculations were made to determine the relative proportions of the path travelled as *Sn* and as *Lg* required to fit the observed travel-times. Velocities of 4.5 and 3.6 km/s were assumed for the mantle and crust, respectively. We also assumed that the 'early *Lg*' phase begins as *Sn* travelling horizontally (shown by the solid lines in profile ARE-north, see Fig. 3). Conversion to *Lg* occurs at an assumed non-horizontal boundary between oceanic mantle and continental crust. Lateral refraction effects at the mantle–crust boundary are assumed to be small so that corrections for this effect are not made. The *Lg* waves then travel directly to the station. The calculated locations of the conversion points shown by the ends of the solid lines are near the region where there is marked crustal thickening. In the region northwest of ARE, crustal thicknesses

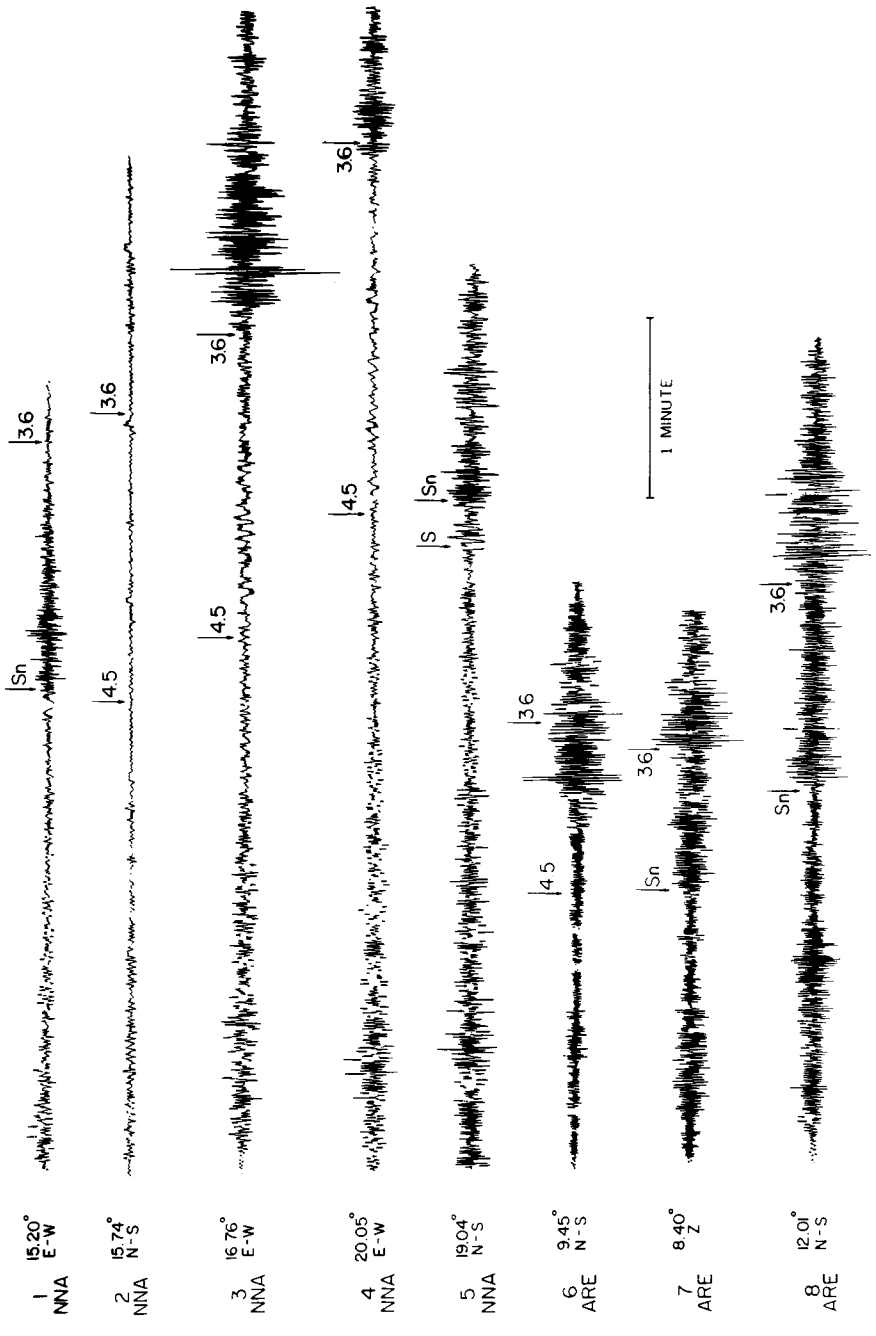

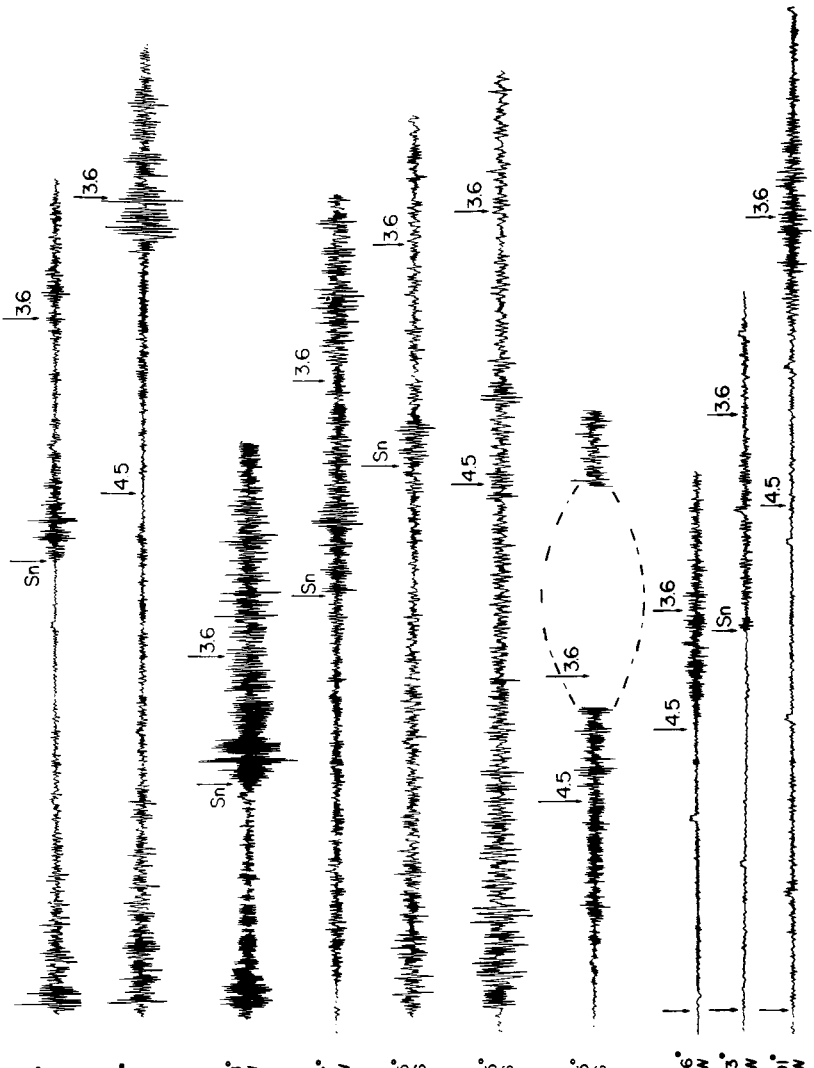

Figure 2. Representative seismograms observed along coastal profiles. Except for event No. 5 which occurred in Colombia, the locations of the events that produced the seismograms are shown in Fig. 3.

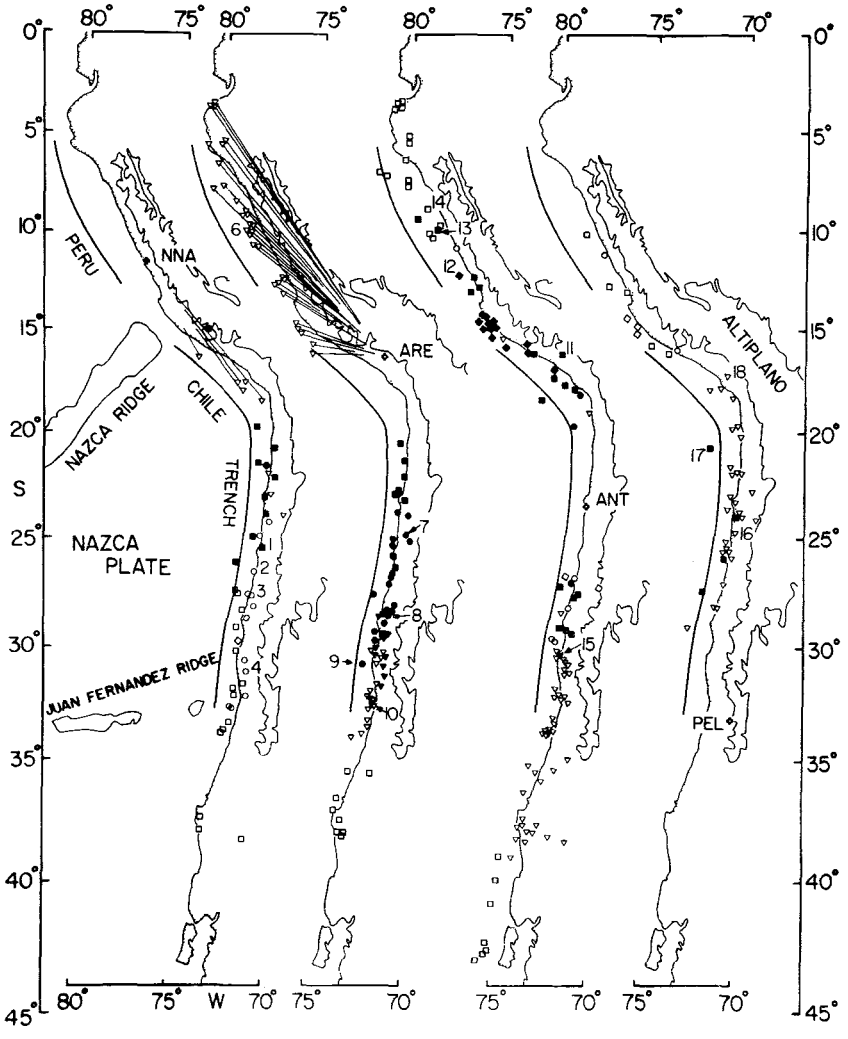

Figure 3. Maps showing the locations of shallow-depth events used in the six coastal profiles: NNA-south, ARE-north, ARE-south, ANT-north, ANT-south and PEL-north. Symbols refer to the classification scheme shown in Table 2. Numbers refer to the seismograms in Fig. 2.

increase from about 7 km in the Nazca plate, to about 14 km beneath the Nazca ridge (Whitsett 1975), about 50 km along the coast, and about 70 km beneath the axis of the Andes (James 1971; Ocola & Meyer 1972). These large gradients in crustal thicknesses from the ocean to the Andes may be responsible for *Sn* to *Lg* conversion. The conversion points are also located near the northern limits of the Altiplano and near the inland projection of the Nazca ridge.

The paths and conversion points in Fig. 3 were calculated under the assumption that lateral refraction effects at the point of conversion are small. However, multipathing effects for surface waves at oceanic–continental transitional regions are sometimes very large (e.g. Capon 1970). For any given event in profile ARE-north, the path along which the 'early *Lg*'

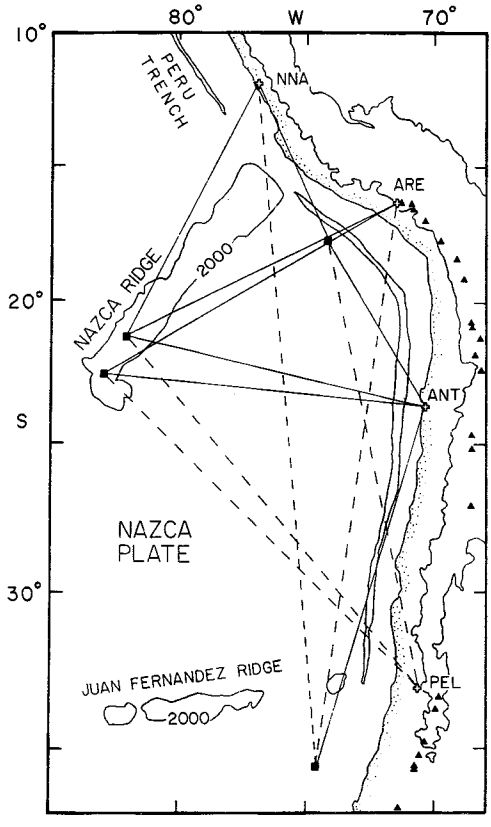

Figure 4. Map showing the pattern of high-frequency shear arrivals in profile NAZCA. Solid lines mean an *Sn* arrival is recorded. Dashed lines mean no high-frequency shear waves are recorded. All stations less than about 15.5° from a source recorded *Sn*, while all stations greater than about 15.5° from a source did not record any high-frequency shear waves.

phases travel may differ significantly from the great circle path. Thus, the conversion could also occur along the coast instead of inland beneath the Altiplano as shown in Fig. 3.

The graph of the corresponding compressional arrivals for profile ARE-north also supports our interpretation of the shear arrival data (Fig. 8). Since the times of the compressional arrivals do not lie along a straight line, they cannot be *Pn* or *Pg* phases. Instead, the scatter in the data may be explained if the arrivals are *Pn* to *Pg* converted phases analogous to the *Sn* to *Lg* converted phases.

Shear arrivals between 5 and 9° in profile NNA-south (Fig. 5) are also similar to the data in profile ARE-north. The arrivals are too slow to be *Sn* and too fast to be *Lg*. The map in Fig. 3 shows that these earthquakes (shown as open inverted triangles) all occur near the region of the bend in the coastline. The great circle paths from the sources to NNA must also cross a region of marked crustal thickening. Calculation of travel-times of the *Sn* to *Lg* conversions similar to those used for profile ARE-north also imply conversion points in the region of crustal thickening southeast of NNA approximately along the inland projection of the Nazca ridge (Fig. 3). 'Early *Lg*' phases are not produced from earthquakes located farther south of the region of the bend in the coastline because paths to NNA are almost totally in the oceanic Nazca plate.

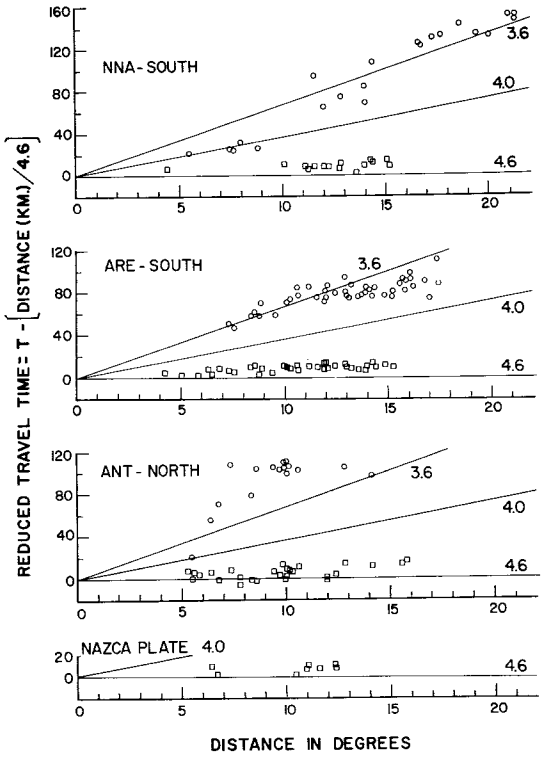

Figure 5. Reduced travel-time versus distance graphs that show high-frequency shear arrivals for four profiles. Squares indicate mantle arrivals (*Sn*). Circles indicate later arrivals ('early *Lg*', *Lg*, or 'late *Lg*').

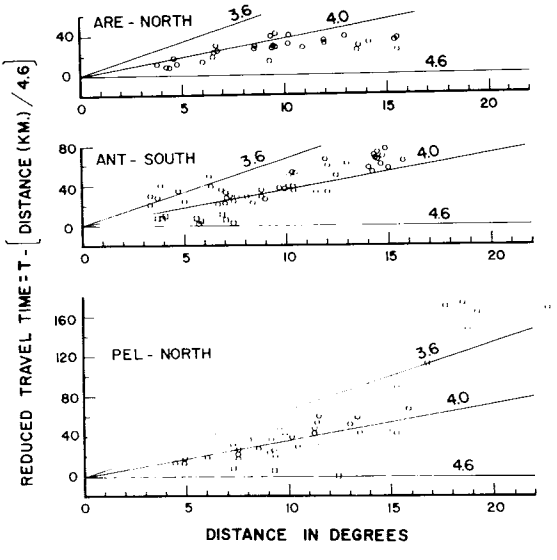

Figure 6. Reduced travel-time versus distance graphs that show high-frequency shear arrivals for three coastal profiles. Symbols are as in Fig. 5.

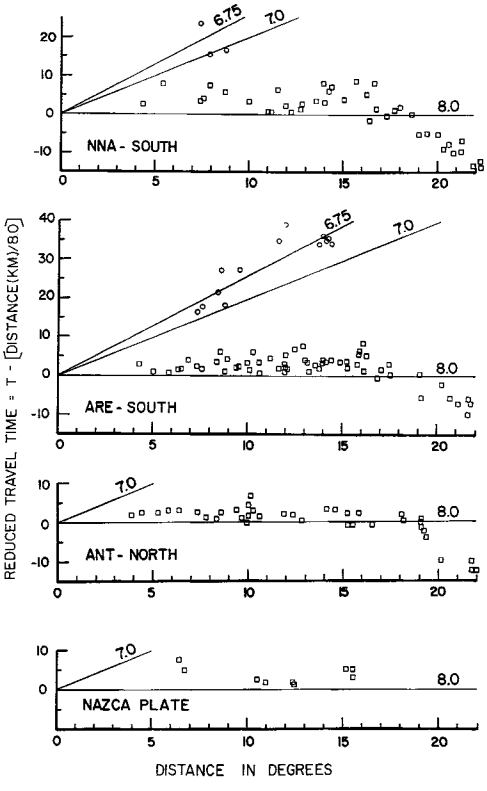

Figure 7. Reduced travel-time versus distance graphs that show high-frequency compressional arrivals for the four profiles used in Fig. 5. Squares indicate first arrivals (probably *Pn* or *P*). Circles indicate second arrivals (probably *Pg*).

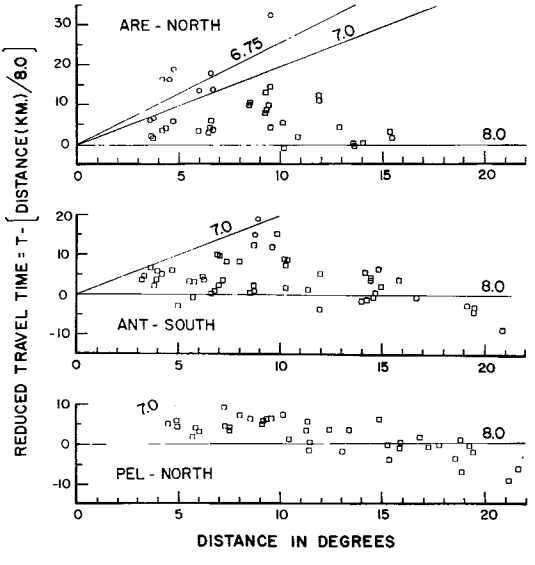

Figure 8. Reduced travel-time versus distance graphs that show high-frequency compressional arrivals for the three profiles used in Fig. 6. Squares indicate first arrivals (probably *Pn*, *P* or converted *Pn* to *Pg* phases). Circles indicate second arrivals (probably *Pg*).

PROPAGATION PATHS ALONG THE CHILEAN MARGIN

It is possible to explain all of the 'early *Lg*' arrivals by the conversion of *Sn* into *Lg* in regions of marked crustal thickening. When calculations were made for the 'early *Lg*' arrivals on profiles ARE-south, ANT-south, and PEL-north (Figs 5 and 6), no simple pattern of conversion points was found as in profiles ARE-north and NNA-south. Instead of clustering in one local region, the conversion points are widely scattered up and down the Chilean coast. In this region, the gradient of crustal thickness is perpendicular to the trench axis, the coastline, and the structural grain of the Andes (James 1971). A careful examination of the geometry for these three profiles shows that the paths, which need not be great circles, lie approximately perpendicular to this gradient or approximately parallel to the Andes. In plane geometry, the intersection point of two nearly perpendicular lines changes position very little when one line is slightly shifted. If, however, the two lines are nearly parallel, a small shift in one line will produce a significant change in the position of the intersection point. Since the conversion points in our model depend on changes in crustal thicknesses, the near-parallel geometry of the propagation paths and the structural grain of the Andes might explain the wide scatter in the calculated conversion points.

For 'early *Lg*' arrivals travelling approximatley parallel to the Chilean coast, *Sn* to *Lg* conversion can be distinguished from *Lg* to *Sn* conversion. If two stations both record an 'early *Lg*' phase produced by the same earthquake, then the interval velocity of the phase is approximately calculated by dividing the difference in the great circle path distances from the earthquake by the difference in the travel-times of the phase observed at the stations. A more refined calculation would correct for any deviation of the actual paths from the assumed great circle paths. Table 3 shows the results of calculations for some station pairs. The range in interval velocities obtained indicates that *Lg* is the phase arriving at the receiving end of the path. Therefore, the type of conversion occurring must be *Sn* to *Lg* and not *Lg* to *Sn*. No *Lg* to *Sn* conversion was ever observed.

That only *Sn* to *Lg* conversion is observed, and not *Lg* to *Sn*, for these paths, can be qualitatively understood using the waveguide model of the two phases. Oceanic *Sn* travels in the waveguide of the Nazca plate lithosphere while continental *Lg* travels in the waveguide of the Andean crust. Since oceanic crust is thin compared to continental crust, there will be a large gradient in crustal thickness along the Chilean coast. If an oceanic *Sn* phase impinges on this dipping crust–mantle boundary at the continental margin, the shallow portion of the *Sn* energy can be transmitted into the crust producing *Lg*. However, if a

Table 3. Summary of interval velocities between station pairs for 'early *Lg*' phases produced by the same earthquake.

Station Pair	Date of Earthquake	Interval Velocity (km/sec)
ANT-PEL (from south)	11/30/64	3.9
	1/14/66	3.7
	10/30/70	3.9
ARE-ANT (from south)	10/14/65	3.5
	11/27/67	3.5
	9/19/70	3.8
PEL-ANT (from north)	6/ 7/66	3.5
	11/29/71	3.4
NNA-ARE (from south)	4/10/66	3.2
	12/29/66	3.3
	9/26/67	3.0
	2/ 6/68	3.2

continental *Lg* phase impinges on this margin, it will not produce *Sn* since energy is not transmitted to the lower parts of the oceanic lithosphere.

For sources in profile ARE-north (Fig. 3), all of the *Sn* energy appears to convert into *Lg* energy. No *Sn* phase was recorded with an 'early *Lg*' phase on the same record. In contrast, for profiles ARE-south, ANT-south and PEL-north (Fig. 3), the near parallel geometry of the propagation paths and the structural grain of the Andes seems to permit some of the *Sn* energy to propagate to the station, while some of it converts into *Lg*. Thus, a 'weak *Sn*' phase in addition to an 'early *Lg*' phase was sometimes recorded on these profiles (see seismogram No. 15 in Fig. 2).

PROPAGATION PATHS AROUND THE BEND REGION IN THE COASTLINE BETWEEN PERU AND CHILE

The graphs of profiles ANT-north (Fig. 5) and PEL-north (Fig. 6) both have many data points with velocities much slower than an *Lg* or *Sg* velocity. Furthermore, the great circle paths of the 'on time *Lg*' phases in profile NNA-south (Fig. 5) are almost completely oceanic. If *Lg*/*Sg* does not propagate in oceanic crust, then the actual paths of these 'on time *Lg*' phases cannot be the great circle path. The 'late *Lg*' arrivals on profiles ANT-north and PEL-north, and the 'on time *Lg*' arrivals on profile NNA-south all have the common attribute that the source is on one side of the bend in the South American coastline near 17° S, while the receiver is on the other side. Let us assume that the actual paths of these 'late *Lg*' and 'on time *Lg*' phases are always approximately parallel to the structural grain of the Andes and curve with the coastline at 17° S. This assumption lengthens the path from the great circle distance. Then the 'on time *Lg*' phases become 'early *Lg*' phases, whereas the 'late *Lg*' phases become 'on time *Lg*' phases or even 'early *Lg*' phases. The existence of 'early *Lg*' phases for our assumed lengthened paths again implies that conversion of *Sn* to *Lg* or *Lg* to *Sn* is occurring.

As before, calculations were made to determine what portion of the lengthened paths must be *Sn* and what portion must be *Lg* to fit the observed 'early *Lg*' arrival times. For example, earthquake No. 4 on profile NNA-south in Fig. 3, which recorded an 'on time *Lg*' is located at a distance of 20.1° from NNA along the great circle path. If the actual path of the phase is assumed to be approximately parallel to the coast of Chile until the bend region and then approximately parallel to the coast of Peru to NNA, the length will be about 22.5°. In order for the calculated arrival time of the 'early *Lg*' phase to fit the observed arrival time, the phase must travel 12.8° as *Sn* and 9.7° as *Lg*. Since only *Sn* to *Lg* conversion has been previously observed, it is reasonable to assume that this same type of conversion is occurring in this case. The bend region is about 13° north of the location of earthquake No. 4 and about 10° southeast of NNA (Fig. 3). The conversion of *Sn* into *Lg* would occur where the crust thickened from ocean to continent. Similar results were obtained for the other 'on time *Lg*' arrivals observed on profiles NNA-south. For the 'on time *Lg*' and 'late *Lg*' arrivals observed on profiles ANT-north and PEL-north, calculations were made for sources located on the Peruvian coast. It is possible that these phases consist of *Sn* travelling southeast to the bend region where they then convert into *Lg* and travel south to the station.

Although this explanation for these 'on time *Lg*' and 'late *Lg*' phases seems plausible, the change in direction of the *Lg* phase from the initial direction of the *Sn* phase cannot be simply explained as lateral refraction according to Snell's law. If Snell's law were obeyed, an *Sn* phase travelling northward from Chile should, after striking the Andean crust near the bend region, travel northeast toward the interior of South America instead of northwest towards NNA.

Sn propagation in the Nazca plate

VELOCITIES

Having explained the arrivals in Figs 5 to 8 that do not approximately lie on straight lines as *Sn* to *Lg* and *Pn* to *Pg* converted phases, we now analyse the arrivals that do approximately lie on straight lines. Since the great circle paths for these arrivals lie mainly in the Nazca plate (Fig. 3), we interpret the shear arrivals to be oceanic *Sn* and the compressional arrivals to be oceanic *Pn* (Figs 5 and 7). The velocities and intercept times are given in Table 4. The compressional arrivals in Fig. 7 lie on a straight line until about 16° where they begin to arrive with velocities greater than 8.0 km/s. We interpret these faster arrivals to be the normal mantle *P* phase. The intercept times in Table 4 have dubious significance. The confidence intervals of the values are large. Also, there may be systematic errors in origin time and epicentre location.

Table 4. *Sn* and *Pn* least squares velocities and intercept times with 95 per cent confidence intervals.

Profile	Sn Velocity (km/sec)	Sn Intercept Time (sec)	No. of Sn Arrivals	Pn Velocity (km/sec)	Pn Intercept Times (sec)	No. of Pn Arrivals
NNA-south	4.51±0.11	2.2±7.8	15	7.98±0.22	-2.0±6.3	16
ARE-south	4.48±0.05	1.3±3.1	36	7.90±0.10	1.2±1.9	42
ANT-north	4.44±0.12	-4.1±6.7	28	8.05±0.10	3.7±2.0	30
NAZCA	4.53±0.24	2.6±13.7	9	8.12±0.29	5.6±5.8	9
All of above	4.46±0.05	-1.1±3.0	88	7.95±0.08	2.0±2.9	97
NNA-south (intermediate depth)	4.67±0.12	11.0±5.5	30	8.28±0.15	6.2±2.4	45
ARE-south (intermediate depth)	4.70±0.09	8.4±3.9	36	8.16±0.12	3.4±1.8	36

Similar reduced travel-time versus distance graphs and velocity-intercept time calculations were made for profiles NNA-south and ARE-south using intermediate-depth (70 to 300 km) earthquakes (Figs 9 (a), (b) and Table 4). The *Sn* and *Pn* velocities are higher than those calculated from shallow-depth earthquakes. This is probably due to the waves sampling higher velocity material at greater depths as well as the effect of source depth on the travel-time curves. The larger intercept times are at least partially due to the greater depths of the sources.

DISAPPEARANCE OF *Sn* AT DISTANCES GREATER THAN ABOUT 16°

Further examination of Figs 3 and 5 shows that oceanic *Sn* is not observed at distances greater than 16° on profiles NNA-south, ARE-south, and ANT-north for the earthquakes examined. These events have body-wave magnitudes (mb) between 4 and 6. The rapid disappearance of the phase between 15 and 16° on all three profiles is very pronounced (see seismograms in Fig. 2). This effect cannot be explained by the presence of any structural features in the oceanic plate that might strongly attenuate *Sn* which are located between 15 and 16° from each of the stations. *Sn* is no longer recorded from sources south of latitude 26.5° S in profile NNA-south, south of 32° S in ARE-south, or north of 11° S in ANT-north. Although *Sn* waves must cross the Nazca ridge in profiles NNA-south and ANT-north, it appears that the ridge has no effect on *Sn* propagation. Furthermore, the pattern of high-frequency shear wave arrivals produced by sources in the Nazca plate seaward of the trench

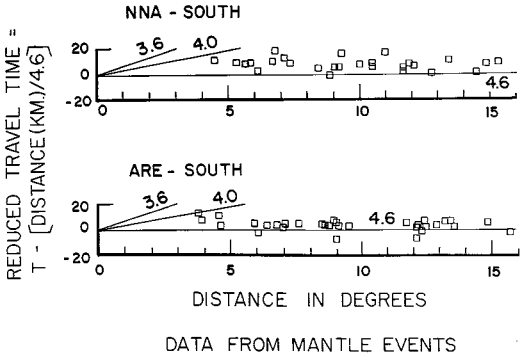

Figure 9(a). Reduced travel-time versus distance graphs that show high-frequency shear arrivals from intermediate-depth events along two coastal profiles. Squares indicate mantle arrivals (*Sn*).

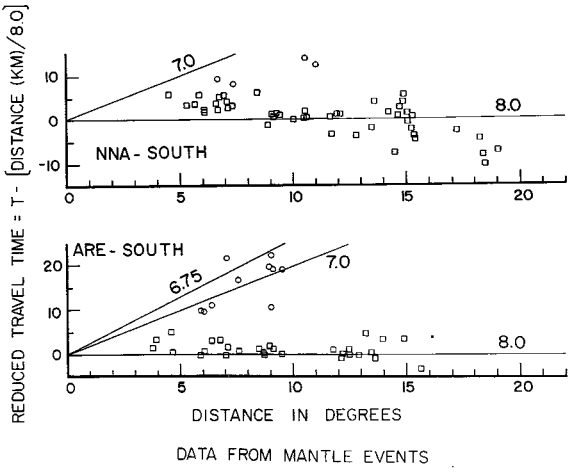

Figure 9(b). Reduced travel-time versus distance graphs that show high-frequency compressional arrivals from intermediate-depth events on two coastal profiles. Squares indicate first arrivals (probably *Pn* or *P*). Circles indicate second arrivals (probably *Pg*, or *Pn* to *Pg* converted phases).

(profile NAZCA) is also characterized by the absence of *Sn* from all sources greater than about 16° away from a recording station (Fig. 4). The sharp disappearance of *Sn* also cannot be explained by coincidental changes in the magnitudes of the sources between 15 and 16°, i.e. by the magnitudes of all the sources located more than 16° away being smaller than those less than 16° away. In some cases *Sn* was recorded at distances of about 15° from magnitude 5.5 sources, whereas *Sn* was not recorded at distances of about 16° from magnitude 6 sources. Finally, the sharp disappearance of *Sn* does not seem to be related to the source orientation relative to the receiving station. The focal mechanism solutions along Peru and Chile show thrust faulting with slip vectors approximately perpendicular to the coastline (Stauder 1973; Stauder 1975). Since *Sn* disappears sharply on three different profiles, which all have different source-receiver orientations, the alignment of nodal planes of *Sn* radiation for all sources greater than 16° is an extremely unlikely explanation for this disappearance phenomenon (Fig. 3).

Therefore, we conclude from the data in these four profiles that *Sn* is observed on short-period components of the WWSSN at distances less than about 15.5° but is severely attenuated at distances greater than about 15.5° along the western coast of South America and in the oceanic Nazca plate. This *Sn* cutoff phenomenon appears to be only a function of path length. Because of the limited number of sources in profile NAZCA, however, the farthest *Sn* recorded in the oceanic Nazca plate travelled only 12.5°. The phase might possibly disappear over a distance of 3° between 12.5 and 15.5° in profile NAZCA instead of the 1° between 15 and 16° found for the three coastal profiles. Thus, it is possible that a sharp cutoff occurs only along the coastal paths landward of the trench, whereas a gradual disappearance of *Sn* occurs for oceanic paths seaward of the trench. The coastal paths for our profiles are not strictly oceanic, but rather lie in the transition region from oceanic to continental crust.

It is difficult to account for this rapid disappearance of *Sn* over a distance of about 1° in a medium characterized by an attenuation mechanism that is independent of frequency (e.g. Carpenter 1966). The decrease in seismic wave amplitude with distance for a constant Q medium is given by

$$\text{ampl.} \propto \exp(-f/f_c)$$

where $f_c = Q/(\pi t)$ and t is the total travel-time of the waves. f_c can be interpreted as a corner frequency whereby the oceanic lithosphere acts as a low pass filter. The frequency responses of short-period WWSSN instruments are peaked at about 1 Hz. Since *Sn* with frequencies of about 1 Hz is clearly recorded from events 15.5° away, f_c cannot be much less than 1 Hz. Therefore, we calculate

$$Q \geq f_c \pi t$$
$$\geq 1200.$$

For a Q of 1000, a change in distance of 1° yields only about a 7 per cent decrease in seismic wave amplitude, whereas a Q of 2000 yields only about a 4 per cent decrease for 1 Hz waves. Such slow decrease in seismic wave amplitude per degree distance cannot account for the sharp cutoff of *Sn* at about 15.5°.

A ray-theory model of *Sn* that does not allow for reflections but only direct rays offers a possible explanation for the cutoff phenomenon. If the oceanic lithosphere can be approximated as a high-Q spherical shell of constant velocity V, then the travel-time (t) versus distance (Δ) relation for surface focus events is

$$t = 2R \sin(\Delta/2)/V$$

where R is the radius of the earth. The maximum penetration depth (D) of the waves will be

$$D = R(1 - \cos(\Delta/2)).$$

In this ray-theory model, *Sn* will be attenuated when the rays penetrate the low-velocity zone. An observed cutoff distance of *Sn* for surface focus events at 15.5° implies that the depth to the top of the low-velocity zone is about 62 km. For deeper sources, the calculated depth to the top of the low-velocity zone would also be greater. If the rays were allowed to reflect at the surface, then the *Sn* waves could travel farther than 15.5° in a manner analogous to the whispering gallery effect (Rayleigh 1945). Since the paths for the coastal profiles lie in the transition region between oceanic and continental crust (Fig. 3), perhaps there are too many structural complexities in the transition region crust to allow efficient reflections to occur.

This ray-model, in which no reflections are allowed, may not apply to the disappearance of *Sn* in the oceanic profile NAZCA. The data in profile NAZCA require only that the phase disappears over a distance of 3°. If the average Q of the Nazca plate is 1000, then a change in distance of 3° will result in a decrease of about 20 per cent in seismic wave amplitude which may be enough to explain the phase's disappearance along oceanic paths.

COMPARISONS WITH OTHER REGIONS: EFFECTS OF THE AGE OF THE LITHOSPHERE

The results of the previous sections show that *Sn* in the 1–2 Hz frequency bandwidth is observed at a maximum distance of about 15.5° and travels with a velocity of about 4.5 km/s in the Nazca plate along the western margin of South America. These results are compared with *Sn* data from other parts of the world in Tables 5 to 7. The literature was searched for reports of *Sn* velocities in other regions. Where possible, a maximum distance for *Sn* observations was estimated from the data given in the literature, or by our examination of short-period WWSSN seismograms of earthquakes in the appropriate regions. Published studies generally report *Sn* velocities but do not consider *Sn* attenuation as a function of distance. Thus, we do not know whether *Sn* disappears gradually in those regions or rapidly as it does along the coast of western South America. The approximate age of each region was also taken from the literature.

Table 5 shows *Sn* data in the 1–2 Hz frequency bandwidth collected from other oceanic regions. Two plausible conclusions can be drawn from this table. Firstly, the maximum distance for which *Sn* is observed tends to increase with the age of the oceanic plate. Secondly, the velocity of *Sn* also tends to increase with the age of the oceanic plate. This second conclusion agrees with the results, for example, of Hart & Press (1973) for regionalized sections of the North Atlantic.

Table 6 shows *Sn* data in the 1–10 Hz frequency bandwidth collected by Walker & Sutton (1971), Sutton & Walker (1972) and Walker (1977). For paths in the oceanic, western Pacific plate, the maximum distance for which *Sn* is observed increases with frequency. For paths crossing the Ontong Java plateau, only *Sn* in the 10 Hz frequency bandwidth is

Table 5. Summary of *Sn* data in the 1–2 Hz frequency bandwidth for various oceanic regions.

Oceanic Region	Approximate Age(m.y.B.P.)	Maximum Observed Distance(°)	Velocity (km/sec)	Age Data*	Seismic Data
Coral Sea	45	<15	no Sn	Gardner (1970)	Barazangi et al. (1978)
North Atlantic (central region)	50	?	4.58	Hart and Press (1973)	Hart and Press (1973)
Nazca Plate (along western South America)	50	15–16	4.48	Herron and Hayes (1969)	This study
Tasman Sea	60–80	13–18	4.55	Hayes and Ringis (1973)	Molnar and Oliver (1969)
Western Pacific (along Tonga–Kermadec arc)	100	≥25	4.75	Larson and Chase (1972)	Aggarwal et al. (1972), and this study
Northwest Pacific	130–160	≥20	4.77	Sutton and Walker (1972)	Sutton and Walker (1972)
Western Atlantic	135–160	≥25	4.72	Heezen and Fornari (1977?)	Isacks and Stephens (1975)

* all in conjunction with map by Heezen and Fornari (1977?)

Table 6. Summary of *Sn* data reported by Sutton & Walker.

Oceanic Region	Approximate Age(m.y.B.P.)	Maximum Observed Distance(°)	Velocity (km/sec)	Peaked Response of Instruments (Hz)	Source
Ontong Java Plateau	60–130	< 15	no Sn	1	Sutton and Walker (1972)
		< 15	no Sn	3–8	Walker and Sutton (1971)
		≥ 20	4.70	10	Walker (1977)
Northwest Pacific Basin	130–160	≥ 20	4.77	1	Sutton and Walker (1972)
		≥ 32	4.79	3–8	Walker and Sutton (1971)
		≥ 37	4.77	10	Walker (1977)

observed. Walker, McCreery, Sutton & Duennebier (1978) conclude that in the 1–10 Hz frequency bandwidth the higher frequencies propagate more efficiently than the lower frequencies so that Q is not independent of frequency for oceanic *Sn*. Although the magnification of the instruments with peaked responses at 10 Hz was about 10 times that of instruments with peaked responses at 1 Hz, this factor still cannot account for the observations of 10 Hz waves at distances of 17° farther than 1 Hz waves (Table 6) for a frequency independent Q.

Table 7 shows *Sn* data in the 1–2 Hz frequency bandwidth collected from continental regions. The data show that *Sn* can be observed over much longer distances in continental regions than in even the oldest oceanic regions. Thus, we conclude that *Sn* in this frequency bandwidth propagates more efficiently in continental than oceanic regions.

The previous conclusions can be qualitatively understood in terms of Stephens & Isacks' (1977) model of *Sn* as it is affected by the thickening of the oceanic lithosphere with age. If the attenuation of *Sn* is primarily due to particle motion in the low-velocity zone beneath the lithosphere, then 1–2 Hz waves travelling in thick oceanic plates will be less affected by the low-velocity zone than will 1–2 Hz waves travelling in thin oceanic plates. Similarly, the greater distances over which *Sn* is observed in continental regions (Table 7) can be explained by the greater thicknesses of continental lithosphere compared to oceanic lithosphere (e.g. Alexander 1974; Jordan 1975). This effect is shown in seismogram No. 5 of Fig. 2. This seismogram is from a Colombian intermediate-depth event which occurred 19° away from NNA. Both the *Sn* and the normal *S* phase are clearly observed. Along this continental path, the lithosphere may be twice as thick as that for the adjacent oceanic Nazca plate, thus allowing for *Sn* to be observed over longer distances.

Furthermore, attenuation as a function of lithospheric thickness accounts for the apparently anomalous results obtained by Molnar & Oliver (1969) who observed *Sn* crossing only part of the oceanic lithosphere beneath the Tasman Sea and not crossing the Coral Sea region at all. Barazangi *et al.* (1978) obtained the same results for the Coral Sea region in a more recent and detailed study. A re-examination of Molnar & Oliver's data shows that *Sn* was observed crossing the Tasman Sea only on the shortest paths. Thus, a relatively thin

Table 7. Summary of *Sn* data in the 1–2 Hz frequency bandwidth for various continental regions.

Continental Region	Maximum Distance Observed(°)	Velocity (km/sec)	Sources
African Shield	≥ 26	4.55–4.72	Gumper and Pomeroy (1970)
India	≥ 27	4.72	Huestis et al. (1973)
Western Australia	≥ 34	4.75	Huestis et al. (1973)
Russian Platform	≥ 41	4.75	Båth (1966)
Canadian Shield	≥ 42	4.72	Brune and Dorman (1963)

lithosphere in which *Sn* would be rapidly attenuated for these young oceanic regions (Table 5) would explain the absence of *Sn* on longer paths.

That the attenuation of oceanic *Sn* is primarily due to particle motion in the low-velocity zone can also explain why Sutton & Walker observed only 10 Hz waves crossing the Ontong Java plateau (see Table 6). According to the calculations of Stephens & Isacks (1977), waves with higher frequencies travelling in a given oceanic region undergo less attenuation per unit distance than waves with lower frequencies. The young age, and hence smaller thickness, of the plateau relative to the western Pacific plate (Kroenke 1972) is consistent with this explanation.

Therefore, it appears that the *Sn* data in Tables 5–7 can be explained mainly by the increase in lithospheric thickness with age and by the normal mode model of Stephens & Isacks (1977) if attenuation is primarily due to particle motion in the low-velocity zone. However, this explanation does not account for the sharp disappearance of *Sn* at about 15.5° along the western coast of South America. That observation may be related to the particular propagation properties along the coast of South America as suggested in the previous section.

Propagation of high-frequency shear waves through and above the segments of the descending Nazca plate

DETERMINATION OF PROPAGATION PATHS

Seismic waves generated by shallow sub-Andean events (i.e. sources occurring beneath the Andes) must traverse the wedge-shaped region of the mantle above the descending Nazca plate on their way to stations near the coast. If the descending plate has higher velocities (7–10 per cent) than the surrounding mantle, then it may be possible for seismic waves to refract into the plate and thus travel along paths other than those found in horizontally layered media. This is likely to occur in South America because of the relatively shallow dip of the descending Nazca plate. A qualitative assessment of these possibilities is shown in the cross-sections of Fig. 10. Fig. 11 shows in map view the locations of the six vertical cross-sections in Fig. 10 which are typical of those encountered. Fig 12 is an interpretive block diagram of cross-section F (Fig. 10), which includes the region of the tear in the descending Nazca plate located beneath southern Peru. Although any refraction of waves into the descending plate will, in general, cause deviations from great circle paths, the sections are still shown along great circle paths as rough first approximations. These sections are intended to guide interpretations of the data, and to point out the difficulties and possible ambiguities in the interpretation of the data.

EFFICIENT PROPAGATION OF *Sn* FROM SOURCES IN THE BENIOFF ZONE

Figs 13 and 14 show some of the typical seismograms produced by shallow- and intermediate-depth events in the Benioff zone (except for event No. 46 in Fig. 13). Fig. 15 shows the pattern of high-frequency shear arrivals produced by these sources. Almost all of them produced clear *Sn* phases at the stations NNA, PEL, ARE, and ANT located along the coast updip from the hypocentres (see seismograms Nos 19 to 22 in Fig. 13). Cross-sections A and B in Fig. 10 show that the paths to these stations probably lie mainly in the descending Nazca plate. Thus, these observations suggest that the descending plate is continuous down to about 200–300 km, or at least that there is no evidence of a major break in the slab in the regions traversed by *Sn*.

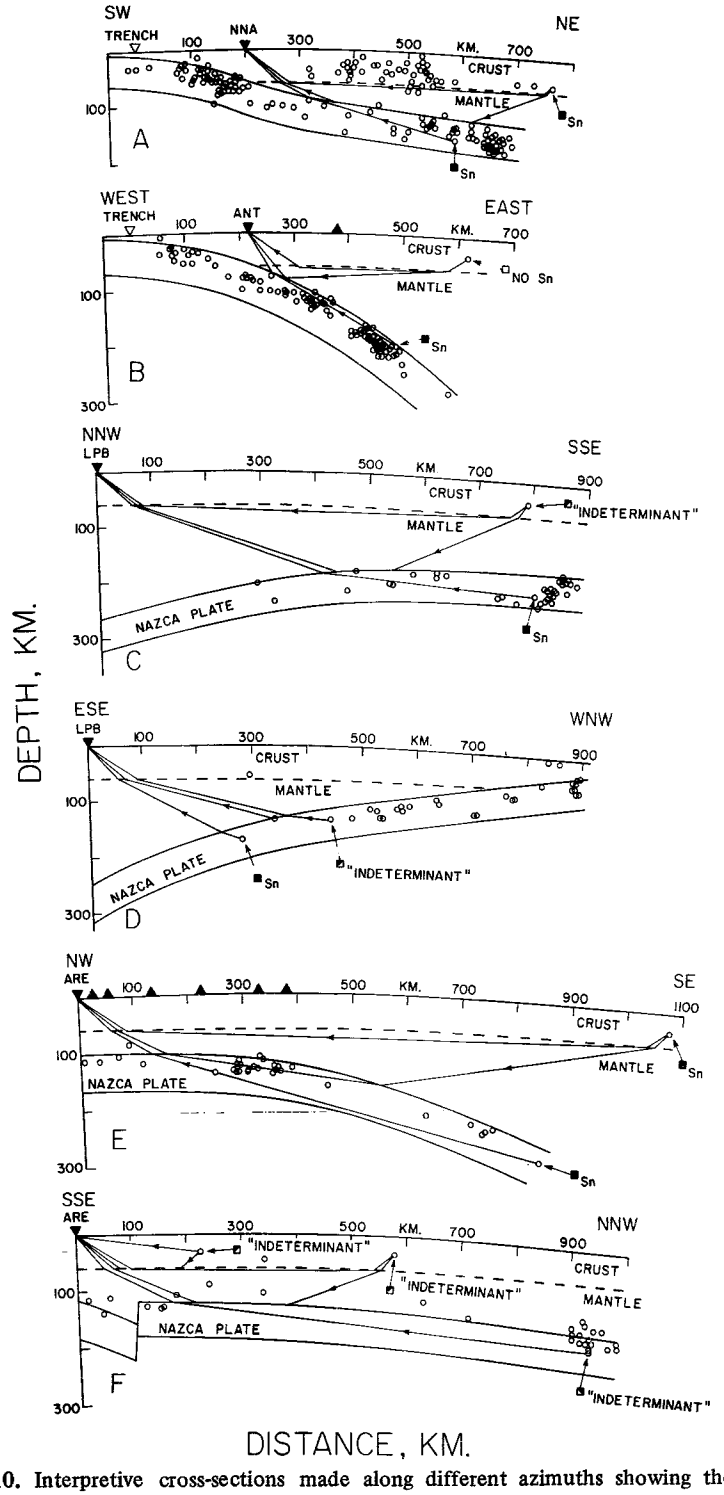

Figure 10. Interpretive cross-sections made along different azimuths showing the geometry of the descending Nazca plate relative to different possible ray paths. The locations of the sections are shown in Fig. 11. The different types of waves produced by some of the sources are represented by symbols shown in Table 2. Upright solid triangles represent active volcanoes.

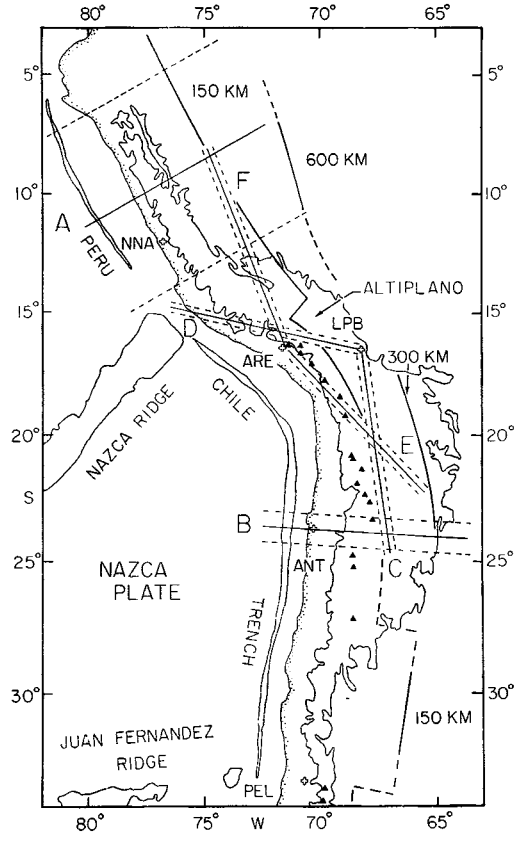

Figure 11. Map showing the locations of the cross-sections of Fig. 10. The heavy solid lines represent the approximate depth to the top of the Benioff zone. Solid triangles represent active volcanoes. The Altiplano corresponds to the widest part of the high Andes shown by the 3 km contour lines.

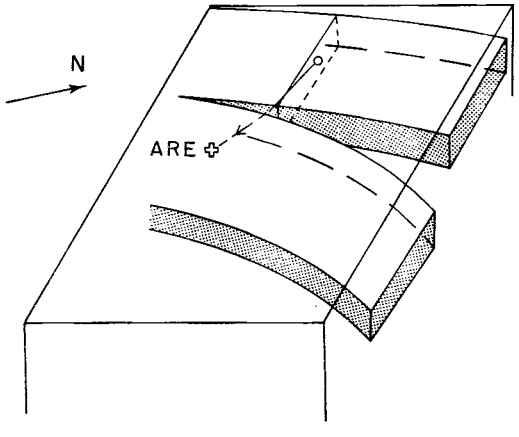

Figure 12. Interpretive diagram of cross-section F in Fig. 10. Waves travelling from sources in Peru to ARE must cross the tear region in the descending Nazca plate.

EFFICIENT PROPAGATION OF *Sn* ALONG PATHS ACROSS THE SHALLOW DIPPING PLATE SEGMENTS

Clear *Sn* phases were also produced by shallow events located in the overriding South American plate. Fig. 16 shows some typical seismograms which record *Sn* waves produced by these sources. Fig. 17 shows, in map view, the paths along which *Sn* efficiently propagated. *Sn* was observed for all paths from shallow sub-Andean events that crossed the regions of central Peru and central Chile in which the Nazca plate has a very shallow dip. Cross-section A of Fig. 10 shows that the paths from the sources to the stations for these events can be either mainly in the uppermost mantle beneath the crust, or in the shallow-dipping descending plate. It is not possible to distinguish between these two paths using travel-time data alone.

If the actual paths are in the uppermost mantle, then the presence of *Sn* implies that the mantle part of the overriding South America plate as well as the wedge-shaped mantle above the shallow-dipping plate segments consist of high-Q material. However, if the actual paths are mainly in the descending plate, and if the plate is overlain by a zone of low-Q material, then the path length of *Sn* through the wedge may be too short to completely attenuate the seismic waves. Thus, the presence of *Sn* along these paths does not yield unambiguous results concerning the attenuation properties of the wedge. Barazangi & Isacks (1976) and Isacks & Barazangi (1977), however, suggest that the correlation of the shallow-dipping plate

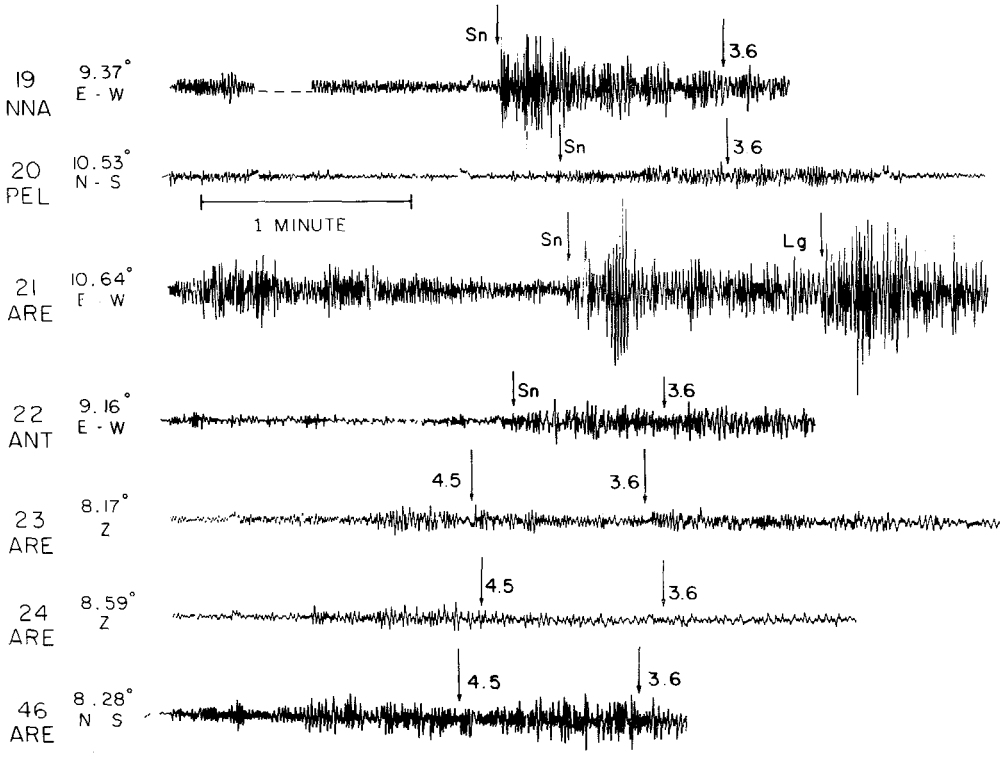

Figure 13. Representative seismograms produced by intermediate-depth events at NNA, PEL, ARE and ANT (except No. 46). The locations of the sources are shown in Fig. 15 (and Fig. 19 for record No. 46). Record No. 46 is produced by a shallow-depth event that is located almost directly above the events that produced records No. 23 and No. 24.

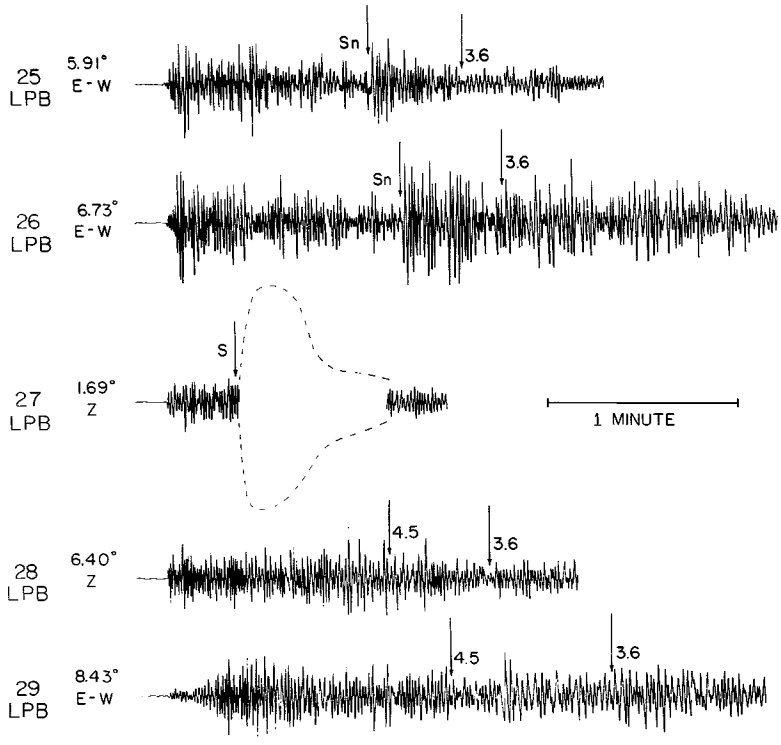

Figure 14. Representative seismograms produced by intermediate-depth events at LPB. The locations of the events are shown in Fig. 15.

segments with regions where there has been no Quaternary volcanism implies that there may be very little or no room for a hot mantle wedge between the overriding and descending plates.

HIGH FREQUENCY SHEAR WAVE PROPAGATION ACROSS THE ALTIPLANO

Propagation paths to Antofagasta (ANT)

High-frequency shear wave propagation across the Altiplano is more complex than that across the shallow-dipping plate segments. In addition to *Sn* phases, low-frequency shear waves, 'indeterminant' waves (i.e. waves which have an indeterminant character), and 'highly scattered' waves are also recorded (Fig. 18). Fig. 19 shows in map view the paths along which these latter three types of waves travelled.

Cross-section B in Fig. 10 shows that waves generated by shallow sub-Andean sources must travel mainly in the wedge of mantle beneath the crust to reach ANT. The dip of the descending Nazca plate is relatively steep so that the waves probably do not refract into the plate to reach the station. Figs 17 and 19 show that *Sn* with a frequency content of about 1 Hz (see seismogram No. 32 in Fig. 16), low-frequency shear waves, and 'indeterminant' waves are observed along paths crossing the Altiplano from shallow sub-Andean events. Furthermore, these two figures show that the paths along which different waves are observed lie very near or are intermingled with one another. Therefore, the mantle wedge in this region is very heterogeneous with respect to high-frequency shear wave propagation. Since

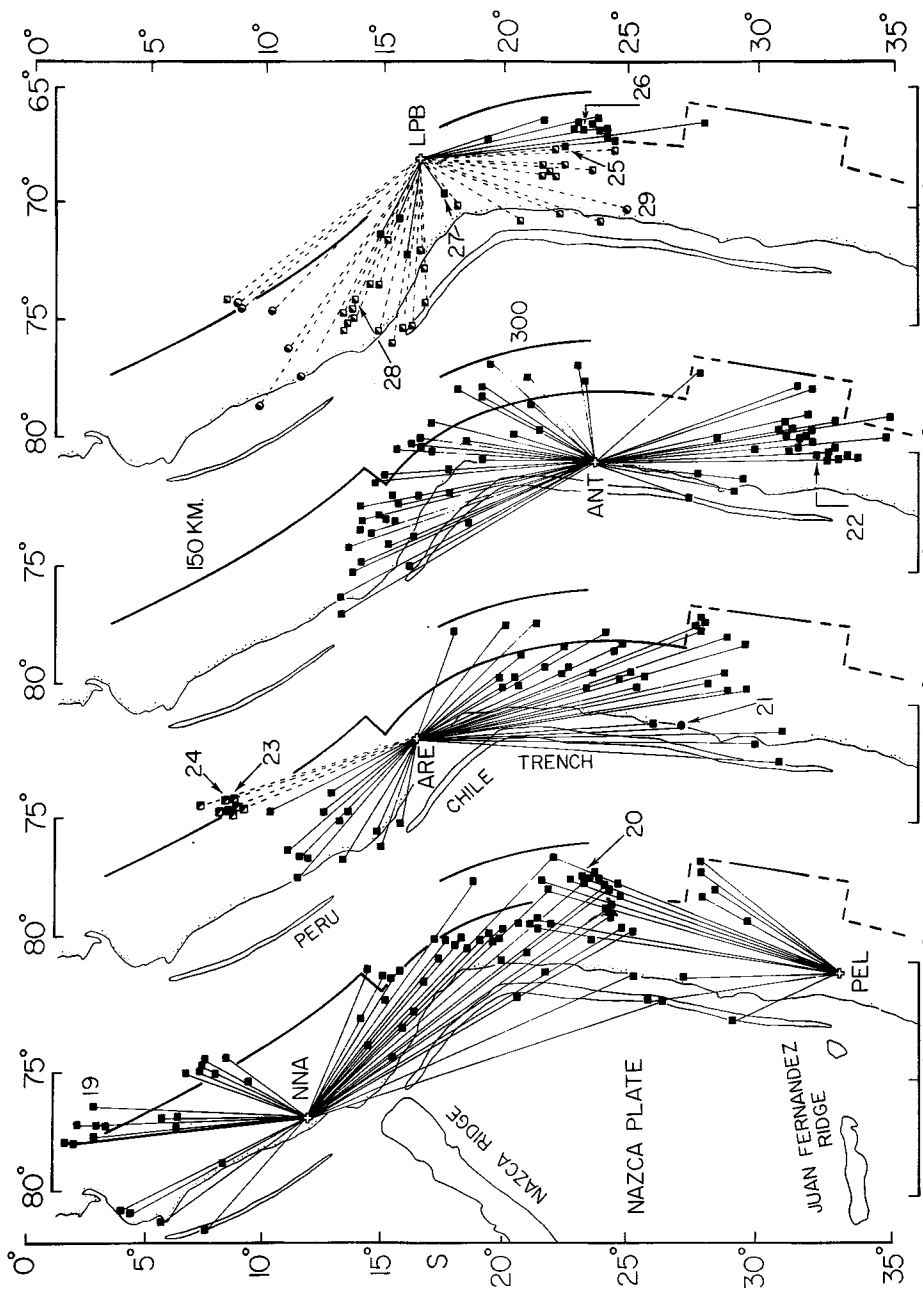

Figure 15. Maps showing the locations of intermediate-depth events used in this study. Symbols refer to the classification scheme shown in Table 2. Numbers refer to the seismograms in Figs 13 and 14. Heavy solid lines represent the depth to the top of the Benioff zone.

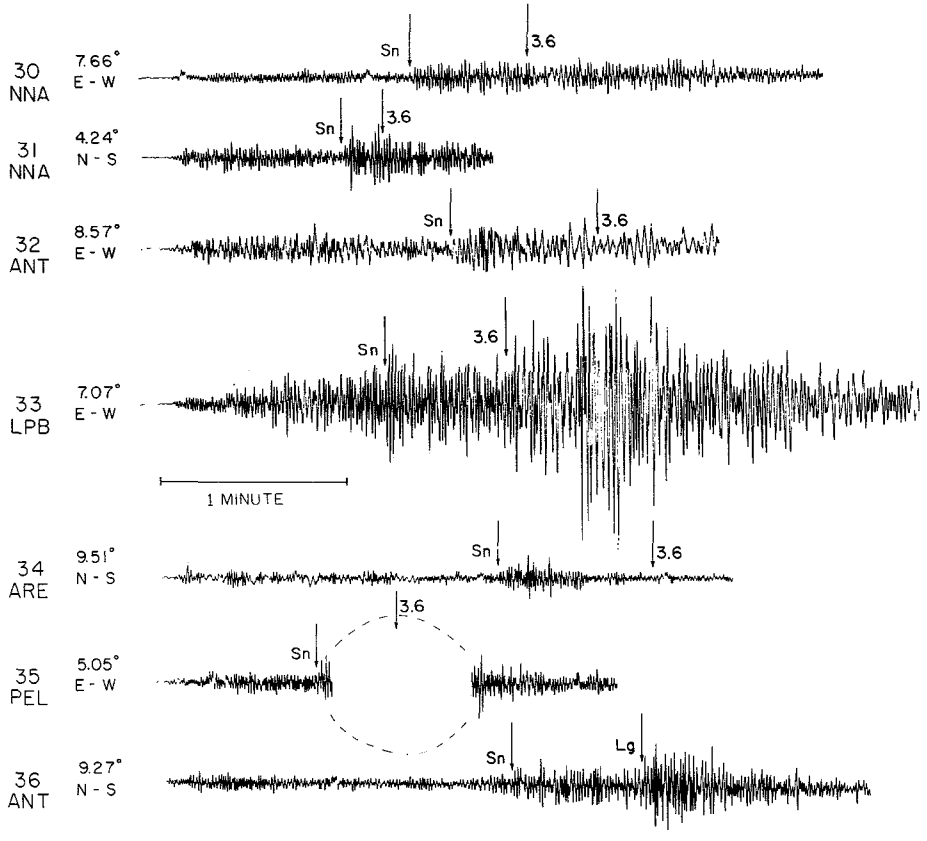

Figure 16. Representative seismograms produced by shallow sub-Andean events and classified as having *Sn*. The locations of the sources are shown in Fig. 17.

high-frequency *Sn* waves are not observed along any of the paths beneath the Altiplano to ANT, the mantle wedge must consist of material that somewhat attenuates, or at least scatters, *Sn*.

Another possible explanation for the absence of *Sn* at ANT is the chance alignments of nodal planes of radiation relative to the receiving station. However, the number of coincidences which need to occur and the correlation of the absence of *Sn* with paths crossing the Altiplano makes this explanation implausible (see left side of Fig. 19).

Propagation paths to Arequipa (ARE)

Fig. 17 shows that *Sn* is observed from shallow sub-Andean sources located southeast of ARE. Along some paths the *Sn* frequency content is relatively high (≥ 2 Hz), whereas along other paths the frequency content is somewhat lower (≤ 1 Hz; see seismogram No. 32 in Fig. 16). This contrast could indicate some variation in Q with change in path azimuth. Cross-section E in Fig. 10 is made along these paths. It shows that the paths between distances of about 100 and 600 km from ARE could possibly be in the descending Nazca plate instead of the mantle wedge. Thus, the observations imply only that *Sn* must propagate efficiently through the mantle wedge farther than about 600 km from ARE along azimuths to the southeast.

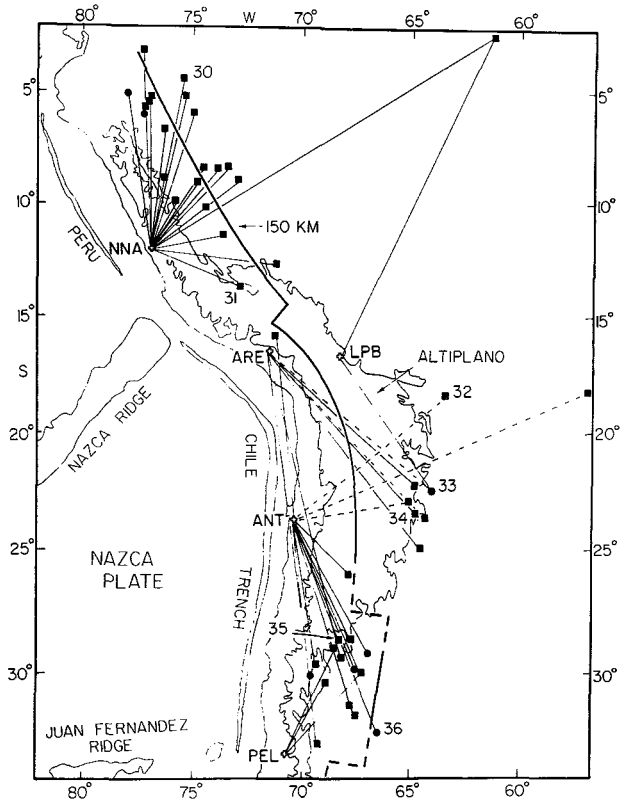

Figure 17. Map showing the locations of shallow sub-Andean events that produced *Sn*. Heavy solid lines represent the depth to the top of the Benioff zone. Symbols refer to the classification scheme shown in Table 2. Numbers refer to seismograms in Fig. 16. Solid lines connecting the events to the stations represent propagation paths along which *Sn* has a frequency content of about 2 Hz. Dashed lines represent propagation paths along which *Sn* has a frequency content of about 1 Hz.

Fig. 19 shows that low-frequency shear waves and 'indeterminant' waves similar to those recorded at ANT are observed along azimuths to the east-southeast of ARE. This figure also shows that 'highly scattered' waves are observed only at ARE. Furthermore, 'indeterminant' waves from both shallow- and intermediate-depth sources to the north-northwest of ARE appear to contain a distinct phase between the expected *Pn* and *Sn* arrival times instead of a gradual build-up of energy (see seismograms Nos 23, 24 and 46 in Fig. 13, and maps in Figs 15 and 19). This phenomenon is not observed at other stations. Cross-section F of Fig. 10, made along an azimuth north-northwest of ARE (see Fig. 11), shows that the waves travelling to ARE must cross the mantle above the inferred tear in the descending Nazca plate. Fig. 12 is an interpretive block diagram of this region. Since these 'highly scattered' waves and a special type of 'indeterminant' waves (classifications No. 11 and No. 12 in Table 2) are observed only at ARE for paths near the tear in the descending plate, we conclude that the mantle above the descending plate north of ARE is very anomalous and a source of severe scattering.

Propagation paths to La Paz (LPB)

Station LPB is located farther inland than the other four stations (Fig. 11). Cross-sections C and D, which are taken along typical paths to the station, must cross a substantial portion

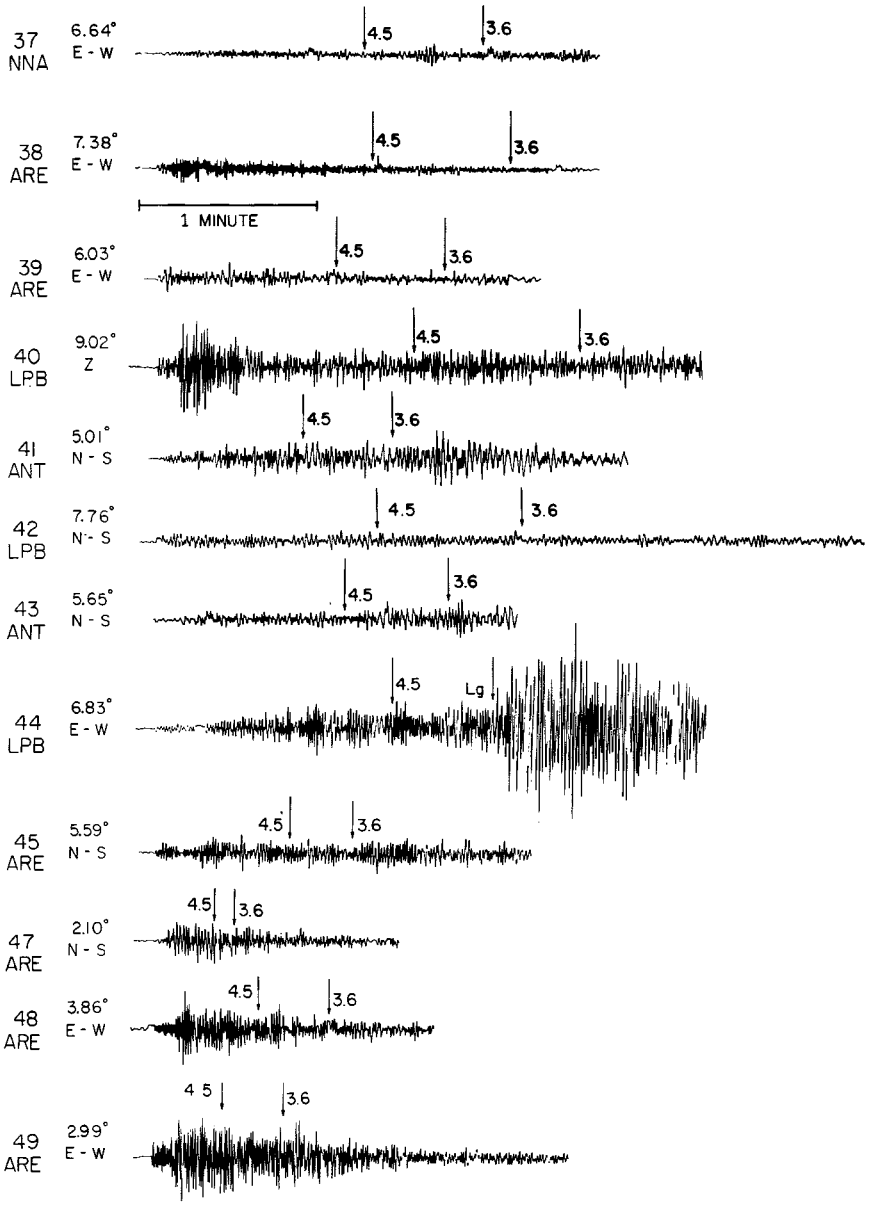

Figure 18. Representative seismograms produced by shallow sub-Andean events. Seismograms Nos 37–43 correspond to symbol 2 in Table 2 (no high-frequency shear arrivals), Nos 44–45 to symbol 10 ('indeterminant' waves), and Nos 47–49 to symbol 11 ('highly scattered' waves). The locations of these sources are shown in Fig. 19.

of the mantle wedge that separates the overriding and descending plates. Typical seismograms of waves recorded at LPB from sources in the Benioff zone are shown in Fig. 14. Fig. 15 shows the pattern of high-frequency shear waves produced by these sources.

Sn is recorded from intermediate-depth sources located to the south-southeast of LPB. As the azimuths of the sources change towards the west, 'indeterminant' waves are recorded

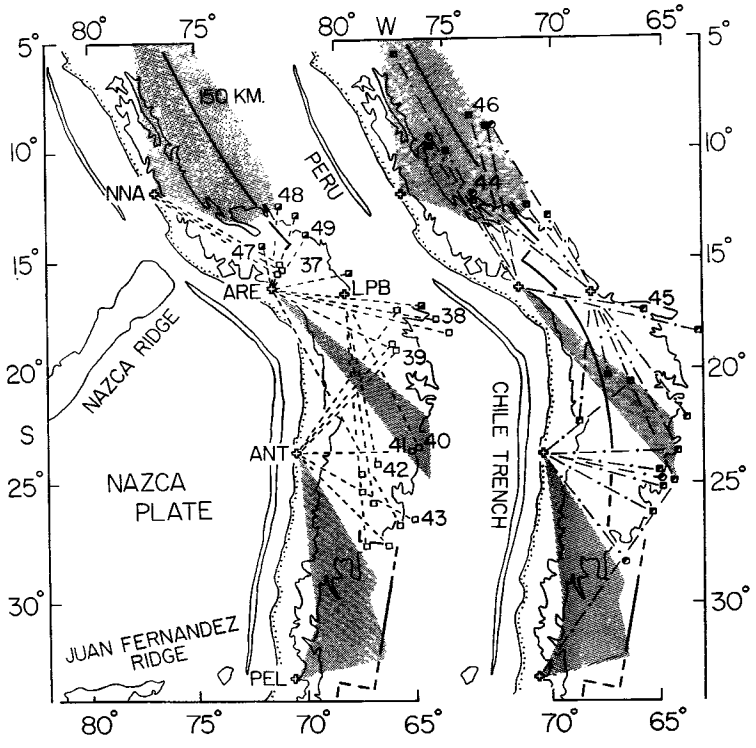

Figure 19. Map showing the locations of shallow sub-Andean events that did not produce high-frequency shear arrivals, that did produce 'indeterminant' waves, or that did produce 'highly scattered' waves. Symbols refer to the classification scheme shown in Table 2. Numbers refer to seismograms in Fig. 19 (and Fig. 13 for record No. 46). Shaded areas indicate regions where *Sn* is observed to propagate efficiently as shown in Fig. 17.

instead. This transition from *Sn* to 'indeterminant' waves is quite sharp (Fig. 15). Cross-section C of Fig. 10 shows the geometry for these southern sources. An azimuthal variation of the properties of the mantle wedge south of the station can explain these observations.

Except for earthquakes with depths greater than 140 km, sources in the Benioff zone west of LPB all produce 'indeterminant' waves (Fig. 15). The geometry of the descending plate in this region is such that the deeper events are located nearer LPB than the shallower events (see cross-section D of Fig. 10). Thus, these observations can be explained by having high-Q material beneath the station and anomalous wedge material farther to the west.

Figs 17 and 19 show the pattern of high-frequency shear waves recorded at LPB from shallow sub-Andean sources. Only low-frequency shear waves and 'indeterminant' waves are observed for paths crossing the Altiplano. *Sn* is observed along one path that crosses the stable continental interior and possibly for another that crosses the eastern edge of the Altiplano (see Fig. 17). However, this latter observation could almost be classified as 'indeterminant' waves rather than *Sn* (see seismogram No. 33 in Fig. 16).

PROPAGATION OF *Lg*

Our data analysis in the previous sections suggests that lateral variations in the efficient propagation of *Sn* are due to lateral variations in the properties of the wedge-shaped

mantle that separates the overriding and descending plates. In a recent study of *Lg* propagation in Asia, Ruzaikin, Nersesov, Khalturin & Molnar (1977) proposed the following three explanations for the absence of *Lg* for paths crossing the Tibetan plateau: (1) abrupt changes in crustal structure at the margins of the plateau, (2) unusual velocity structure beneath the plateau, and (3) the existence of low-Q regions in the Tibetan plateau. However, the analysis of the *Lg* data in this study suggests that the primary factor in the efficient propagation of *Lg* is the orientation of the path relative to the structural trend of the Andes (see circle symbols in Figs 17 and 19). When *Lg* is observed (see also Cabre 1971), the path is approximately parallel to the structural trend of the Andes. The converse, though, is not true because there are many paths that are approximately parallel to the structural trend of the Andes along which *Lg* is not observed. There are only two paths that are approximately perpendicular to the structural trend of the Andes along which Lg is recorded (see right side of Fig. 19). These two paths, however, cross the widest part of the Altiplano. *Lg* was not observed for paths crossing the narrower parts of the Andes.

Since *Lg* is a high-frequency shear phase guided in the continental crust, this phenomenon can be qualitatively explained by variations in the structure of the Andes as opposed to variations in the Q of the crust. *Lg* will efficiently propagate only along paths where the crustal structure is sufficiently uniform, such as along paths parallel to the trend of the Andes and across the widest part of the Altiplano. *Lg* will not propagate along paths where the crust is not relatively uniform, such as along paths perpendicular to the trend of the Andes.

MAPPING LATERAL VARIATIONS IN THE EFFICIENT PROPAGATION OF *Sn*

By using the interpretive cross-sections shown in Fig. 10 and by piecing together the maps in Figs 15, 17 and 19, we constructed a map that can account for all of the variations in high-frequency shear wave arrivals from shallow sub-Andean earthquakes (Fig. 20). The descending plate was considered to be a region of high-Q from the observations of efficient propagation of *Sn* produced by sources located in the Benioff zone. The crust was also considered to be a region of high-Q, since *Lg* was observed to travel efficiently along paths parallel to the structural trend of the Andes. The absence of *Lg* was attributed to effects other than to the presence of low-Q material in the crust (see previous section).

Fig. 20 was then constructed as follows. Firstly, solid lines were drawn in regions where high-frequency *Sn* (1–2 Hz) propagated efficiently (see Figs 17 and 3). Next, dashed lines were drawn in regions where 'indeterminant' waves, low-frequency shear waves, and 'highly scattered' waves were observed (Fig. 19). The paths along which lower frequency *Sn* (≤ 1 Hz) is observed were also included in the dashed regions, since the relatively lower frequencies indicate that some sort of above-normal attenuation occurs along these paths. In the areas where the two regions overlap, only solid lines were drawn. It was assumed that *Sn* propagates efficiently in these areas, since high-frequency waves must efficiently propagate along the whole path if *Sn* is observed, whereas only a small part of the path need be a source of attenuation/scattering if *Sn* is not observed. Thus, the dashed areas represented the maximum possible extent of the regions in the mantle wedge that attenuate/scatter high-frequency seismic waves if the waves do not refract along the upper boundary of the descending plate. These areas could be much smaller and still produce the same observed pattern of high-frequency shear arrivals. Blank regions indicate that there is no information about the mantle properties, either because of lack of data, or because of the occurrence of *Sn* to *Lg* conversion.

Because of the ambiguities involved in determining the paths for shallow sub-Andean events due to the possible refraction of waves through the descending plate, it is possible

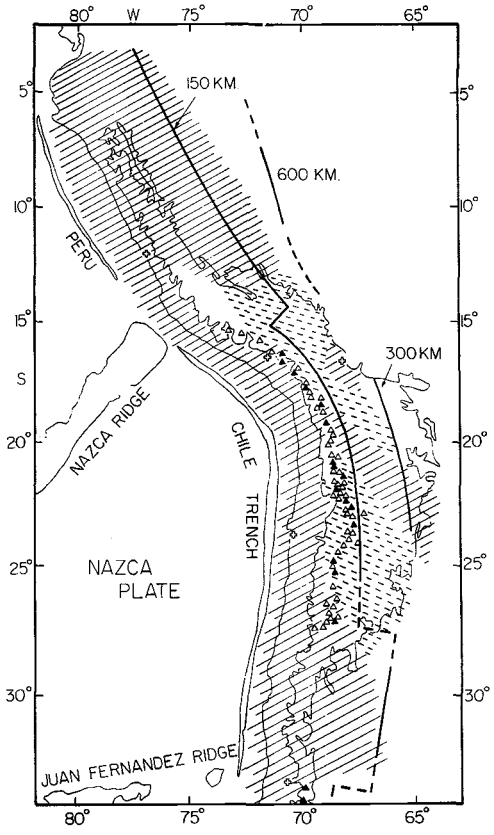

Figure 20. Map showing lateral variations in high-frequency shear wave (mantle) arrivals from shallow sub-Andean events. *Sn* propagates efficiently along the regions represented by the solid lines. Inefficient *Sn* propagation is represented by the dashed lines. Triangles represent active (solid) and recent (open) volcanoes. Heavy solid lines represent the depth to the top of the Benioff zone.

that the solid lines in Fig. 20, representing the mantle above the shallow dipping plate segments and the corridor through the Altiplano to ARE, may actually be due to propagation in the high-Q descending plate. Thus, our mapping has produced somewhat inconclusive results regarding these regions. All that can be stated definitely is that there must be some regions in the mantle wedge, represented by the dashed lines, that attenuate/scatter high-frequency seismic waves. The existence of these regions that attenuate/scatter high-frequency seismic waves is why Molnar & Oliver (1969) could not explain their limited *Sn* data for western South America strictly in terms of continuous or discontinuous lithosphere all along the South American subduction zone.

POSSIBLE GEOLOGICAL IMPLICATIONS

In a study of the Tonga island arc, Mitronovas *et al.* (1969) found considerable variations in the character of seismic waves recorded at stations located on active volcanic ridges compared to waves recorded at stations located on non-volcanic ridges closer to the trench. Seismic phases recorded on non-volcanic ridges tended to be sharp and prominent, whereas those recorded on active volcanic ridges tended to be emergent and drawn-out. Mitronovas

et al. suggested that the emergent character was due to complex and heterogeneous structure beneath the active volcanic ridges.

Variations in seismic wave character suggest that there are three different types of regions in the wedge of mantle in the Tonga island arc region. Firstly, there is the region of extremely hot mantle material beneath the active marginal basin which severely attenuates *P* and *S* waves. Secondly, there is the region beneath the active volcanic arc located trenchward of the active marginal basin through which high-frequency *P* and *S* waves can pass. However, these waves are scattered and are recorded as emergent, drawn-out wavetrains. This could be due to complex and heterogeneous structure beneath the volcanoes. Finally, there is the region beneath the non-active volcanic arc still farther trenchward of the active marginal basin through which sharply-defined high-frequency waves can pass. Thus, there is a transition from a regime in which no high-frequency *S* waves are observed to one in which sharp high-frequency *S* waves are observed.

It is possible that the wedge of mantle beneath the Altiplano does not completely attenuate high-frequency shear waves, as does the material beneath an active marginal basin, but rather partly attenuates and scatters such waves. This would account for the presence of 'indeterminant' and low-frequency shear waves for paths passing beneath the Altiplano. The observations of *Sn* crossing the wedge of mantle beneath the central part of the Altiplano could actually be due to the refraction of high-frequency waves through the descending plate, rather than to the existence of a high-*Q* corridor.

Noble *et al.* (1974) document the occurrence of episodes of intense volcanism and tectonism in the Andes of Peru and around the circum-Pacific belt beginning in the Miocene and ending in the Pleiocene (see also Handschmacher 1976). Thus, the Altiplano could be a result of previous tectonic activity and not the response to present heating of the mantle. If it were the latter, then we might expect to observe the complete attenuation of high-frequency seismic waves for all paths beneath the Altiplano rather than 'indeterminant' waves and a possible high-*Q* corridor.

Conclusions

(1) The efficient conversion of oceanic *Sn* into continental *Lg* readily occurs in many regions along western South America where there are large gradients in crustal thicknesses. This conversion occurs: (1) beneath southern Peru where the crust of the Andes probably thickens near the beginning of the Altiplano, (2) along the continental margin in Chile, and (3) at the region of the bend in the coastline between Peru and Chile.

(2) For propagation paths in the oceanic Nazca plate along western South America, *Sn* has a velocity of 4.5 km/s and is observed up to a maximum distance of about 15.5°. The disappearance of the *Sn* phase occurs quite abruptly for sources with body-wave magnitudes that range from about 4 to 6, and cannot simply be explained by the standard attenuation with distance mechanisms. On a global scale the maximum observation distance of *Sn* increases with the age, and hence thickness, of the oceanic plate in which the phase travels. Efficient propagation of *Sn* is observed for the farthest distances in continental shield regions where the lithosphere is thickest. Along the same oceanic paths, *Sn* in the 10 Hz frequency bandwidth is observed to travel farther than *Sn* in lower frequency bandwidths. Furthermore, the velocity of *Sn* also appears to increase with the age of the oceanic plates. All of these global observations of *Sn* can be qualitatively explained if *Sn* is interpreted in terms of normal modes.

(3) Propagation of high-frequency shear waves through the wedge of mantle above the segments of the descending Nazca plate is very complex. For propagation paths located

mainly in the descending Nazca plate, only *Sn* is observed. However, for paths located even partially in the wedge-shaped mantle that separates the overriding South American plate and the descending Nazca plate, *Sn* is observed as well as low-frequency shear waves, 'indeterminant' waves, and 'highly scattered' waves. The geometry of the descending plate segments is such that it is impossible to infer uniquely the exact locations or boundaries of attenuating/scattering material in the mantle-wedge from lateral variations in high-frequency shear wave propagation. However, it is clear that the regions in the mantle that attenuate/scatter high-frequency shear waves along western South America do exist beneath the Altiplano, the high Andean plateau.

(4) Efficient *Lg* propagation in the Andean crust primarily occurs when the propagation paths are approximately parallel to the structural grain of the Andes.

Acknowledgments

We thank Jack E. Oliver for reviewing the paper; Judy Healey for editorial assistance; Noreen Fitzpatrick, Maria Araceli de Ramos, and Deborah Citron for drafting the figures. This work was supported by the Office of Naval Research Contract No. N00014-75-C-1121. Cornell University, Department of Geological Sciences, Contribution No. 629.

References

Aggarwal, Y., Barazangi, M. & Isacks, B., 1972. *P* and *S* travel-times in the Tonga–Fiji region: a zone of low velocity in the uppermost mantle behind the Tonga island arc, *J. Geophys. Res.*, 77, 6427.

Alexander, S., 1974. Comparison of crust and mantle structure beneath shields and the influence of shield on the dynamics of plate motions (abstract), *EOS, Trans. Am. Geophys. Union*, **55**, 358–359.

Barazangi, M. & Isacks, B., 1971. Lateral variations of seismic-wave attenuation in the upper mantle above the inclined earthquake zone of the Tonga island arc: deep anomaly in the upper mantle. *J. Geophys. Res.*, **76**, 8493.

Barazangi, M., Isacks, B., Dubois, J. & Pascal, G., 1974. Seismic wave attenuation in the upper mantle beneath the southwest Pacific, *Tectonophysics*, **24**, 1.

Barazangi, M., Pennington, W. & Isacks, B., 1975. Global study of seismic wave attenuation in the upper mantle behind island arcs using *pP* waves, *J. Geophys. Res.*, **80**, 1079.

Barazangi, M. & Isacks, B., 1976. Spatial distribution of earthquakes and subduction of the Nazca plate beneath South America, *Geology*, **4**, 686.

Barazangi M., Oliver, J. & Isacks, B., 1978. Relative excitation of the seismic shear waves *Sn* and *Lg* as a function of source depth and their propagation from Melanesia and Banda arcs to Australia, *Annali di Geofisica*, in press.

Båth, M. 1966. Propagation of *Sn* and *Pn* to teleseismic distances, *Pure and Applied Geophysics*, **64**, 19.

Brune, J. & Dorman, J., 1963. Seismic waves and earth structure in the Canadian shield, *Bull. Seis. Soc. Am.*, **53**, 167.

Cabre, R., 1971. Ondas Lg registradas en La Paz, Bolivia, *Geofisica Panamericana*, **1**, 71, (in Spanish).

Capon, J., 1970. Analysis of Rayleigh-wave multipath propagation of LASA, *Bull. Seis. Soc. Am.*, **60**, 1701.

Carpenter, E., 1966. Absorption of elastic waves – an operator for a constant Q mechanism, *At. Weap. Res. Estab.*, Report No. 0-43/66, HMSO.

Dept. of Terrestrial Magnetism staff, 1970. Explosion studies in the Altiplano, *Carnegie Institution Yearbook*, 68, 459.

Duschenes, J. & Solomon, S., 1977. Shear wave travel time residuals from oceanic earthquakes and evolution of oceanic lithosphere, *J. Geophys. Res.*, **82**, 1985.

Forsyth, D., 1975. The early structural evolution and anisotropy of the oceanic upper mantle, *Geophys. J. R. astr. Soc.*, **43**, 103.

Gardner, J., 1970. Submarine geology of the western Coral sea, *Geol. Soc. Am. Bull.*, **81**, 2599.

Gumper, F. & Pomeroy, P., 1970. Seismic wave velocities and earth structure on the African continent, *Bull. Seis. Soc. Am.*, **60**, 651.

Handschmacher, D., 1976. Post-Eocene plate tectonics of the eastern Pacific, in *The Geophysics of the Pacific Ocean Basin and Its Margin,* The Woollard Volume, Geophysical Monograph Series No. 19, p.177, eds G. Sutton, M. Manghnani, and R. Moberly.

Hart, R. & Press, F., 1973. *Sn* velocities and the composition of the lithosphere in the regionalized Atlantic, *J. Geophys. Res.*, **78**, 407.

Hayes, D. & Ringis, J., 1973. Sea floor spreading in the Tasman Sea, *Nature,* **243**, 454.

Heezen, B. & Formari, D., 1977. Geological Map of the Pacific Ocean, *Geological World Atlas*, sheet 10, UNESCO.

Herron, E. & Hayes, D., 1969. A geophysical study of the Chile ridge, *Earth Plan. Sci. Letters,* **6**, 79.

Huestis, S., Molnar, P. & Oliver, J., 1973. Regional *Sn* velocities and shear velocity in the upper mantle, *Bull. Seis. Soc. Am.*, **63**, 469.

Isacks, B. & Molnar, P., 1971. Distribution of stresses in the descending lithosphere from a global survey of focal-mechanism solutions of mantle earthquakes, *Rev. Geophys. Space Phys.*, **9**, 103.

Isacks, B. & Barazangi, M., 1973. High frequency shear waves guided by a continuous lithosphere descending beneath western South America, *Geophys. J. R. astr. Soc.*, **33**, 129.

Isacks, B. & Stephens, C., 1975. Conversion of *Sn* to *Lg* at a continental margin, *Bull. Seism. Soc. Am.*, **64**, 235.

Isacks, B. & Barazangi, M., 1977. Geometry of Benioff zones: lateral segmentation and downwards bending of the subducted lithosphere, in *Island Arcs, Deep Sea Trenches and Back-Arc Basins,* Ewing Series, Vol. I, Am. Geophys. Union.

James, D., 1971. Andean crustal and upper mantle structure, *J. Geophys. Res.*, **76**, 3246.

Jordan, T., 1975. The continental tectosphere, *Rev. Geophys. Space Phys.*, **13**, 1.

Karig, D., 1971. Origin and development of marginal basins in the western Pacific, *J. Geophys. Res.*, **76**, 2542.

Kausel, E., Leeds, A. & Knopoff, L., 1974. Variations of Rayleigh wave phase velocities across the Pacific Ocean, *Science,* **186**, 139.

Kroenke, L., 1972. Geology of the Ontong Java Plateau, *Ph.D. thesis,* Dept. of Geol. and Geophys., University of Hawaii.

Larson, R. & Chase, C., 1972. Late Mesozoic evolution of the western Pacific Ocean, *Geol. Soc. Am. Bull.*, **83**, 3627.

Leeds, A., Knopoff, L. & Kausel, E., 1974. Variations of upper mantle structure under the Pacific Ocean, *Science,* **186**, 141.

Leeds, A., 1975. Lithospheric thickness in the western Pacific, *Phys. Earth and Planet. Int.*, **11**, 61.

Mitronovas, W., Isacks, B. & Seeber, L., 1969. Earthquake locations and seismic wave propagation in the upper 250 km of the Tonga island arc, *Bull. Seism. Soc. Am.*, **59**, 1115.

Molnar, P. & Oliver, J., 1969. Lateral variations of attenuation in the upper mantle and discontinuities in the lithosphere, *J. Geophys. Res.*, **74**, 2648.

Noble, D., McKee, E., Farrar, E. & Petersen, U., 1974. Episodic Cenozoic volcanism and tectonism in the Andes of Peru, *Earth Planet. Sci. Letters,* **21**, 213.

Ocola, L. & Meyer, R., 1972. Crustal low-velocity zones under the Peru–Bolivia Altiplano, *Geophys. J. R. astr. Soc.*, **30**, 199.

Oliver, J., Ewing, M. & Press, F., 1955. Crustal structure of the Arctic regions from the *Lg* phase, *Geol. Soc. Am. Bull.*, **66**, 1063.

Oliver, J. & Isacks, B., 1967. Deep earthquake zones, anomalous structures in the upper mantle, and the lithosphere, *J. Geophys. Res.*, **72**, 4259.

Oxburgh, E. & Turcotte, D., 1970. Thermal structure of island arcs, *Geol. Soc. Am. Bull.*, **81**, 1665.

Rayleigh, Lord J., 1945. *The Theory of Sound,* 2nd Edition, Robert Bruce Linday, New York, 126.

Rial, J., 1976. Seismic-wave transmission across the Caribbean plate: high attenuation on concave side of Lesser Antilles island arc, *Bull. Seis. Soc. Am.*, **66**, 1905.

Ruzaikin, A., Nersesov, I., Khalturin, V. & Molnar, P., 1977. Propagation of *Lg* and lateral variations in crustal structure in Asia, *J. Geophys. Res.*, **82**, 307.

Schmucher, U., 1969. Conductivity anomalies with special reference to the Andes, in *The Application of Modern Physics to the Earth and Planetary Interiors,* ed. S. K. Runcorn, 125.

Sclater, J., Lawver, L. & Parsons, B., 1975. Comparison of long-wavelength residual elevation and free air gravity anomalies in the north Atlantic and possible implications for the thickness of the lithospheric plate, *J. Geophys. Res.*, **80**, 1031.

Snoke, J., Sacks, I. & Okada, H., 1974. A model not requiring continuous lithosphere for anomalous high-frequency arrivals from deep focus South American earthquakes, *Phys. Earth and Planet. Int.*, 9, 199.

Stauder, W., 1973. Mechanism and spatial distribution of Chilean earthquakes with relation to subduction of the oceanic plate. *J. Geophys. Res.*, 78, 5033.

Stauder, W., 1975. Subduction of the Nazca plate under Peru as evidenced by focal mechanisms and by seismicity, *J. Geophys. Res.*, **80**, 1053.

Stephens, C. & Isacks, B., 1977. Towards an understanding of *Sn*: normal modes of Love waves in an oceanic structure, *Bull. Seis. Soc. Am.*, 67, 69.

Sutton, G. & Walker, D., 1972. Oceanic mantle phases recorded on seismographs in the northwest Pacific at distances between 7° and 40°, *Bull. Seis. Soc. Am.*, **62**, 631.

Sykes, L., 1972. Seismicity as a guide to global tectonics and earthquake prediction, *Tectonophysics*, **13**, 393.

Toksoz, M., Sleep, N. & Smith, A., 1973. Evolution of the downgoing lithosphere and mechanisms of deep focus earthquakes, *Geophys. J. R. astr. Soc.*, **35**, 285.

Walker, D. & Sutton, G., 1971. Oceanic mantle phases recorded on hydrophones in the northwestern Pacific at distances between 9° and 40°, *Bull. Seis. Soc. Am.*, **61**, 65.

Walker, D., 1977. High-frequency *Pn* and *Sn* phases recorded in the western Pacific, *J. Geophys. Res.*, **82**, 3350.

Walker, D., McCreery, C., Sutton, G. & Duennebier, F., 1978. Spectral analyses of high-frequency *Pn* and *Sn* phases observed at great distances in the western Pacific, *Science*, **199**, 1333.

Whitsett, R., 1975. Gravity measurements and their structural implications for the continental margin of southern Peru, *Ph.D. thesis*, Dept. of Geophysics, Oregon State University.

Yoshii, T., Yoshiteru, K. & Ito, Y., 1976. Thickening of the oceanic lithosphere, in *The Geophysics of the Pacific Ocean Basin and Its Margin*, the Woolard volume, Geophysical Monograph Series No. 19, p. 423, eds G. Sutton, M. Manghnani and R. Moberly.